UNCLASSIFIED

Australian Government

Department of Defence
Science and Technology

Methods of Designing and Feeding Carbon Fibre Reinforced Plastic Slotted Waveguide Antenna Arrays

Derek Gray, Kelvin J. Nicholson, Paul J. Callus and Kamran Ghorbani

Aerospace Division
Defence Science and Technology Group

DST-Group-TR-3424

ABSTRACT

This report describes the ongoing development of the Slotted Waveguide Antenna Stiffened Structure (SWASS) technology during the period 2010 to 2012. In SWASS, blade stiffeners in sandwich panels or top-hat stiffeners on skins serve the dual purpose of providing both structural reinforcement while acting as radiofrequency waveguides. Slots cut through the outer skin and into the waveguides produce slotted waveguide antenna arrays. The development and validation of a radiofrequency design methodology, based on the finite element method, for resonant slotted waveguide antenna arrays, is described. This methodology was used to design seven-slot and ten-slot arrays that were subsequently machined into waveguides manufactured from aluminium alloy and aerospace grade carbon fibre reinforced plastic (CFRP). Additionally, the performance of a plug-and-loop radiofrequency feeding method for resonant SWASS waveguides is analysed.

RELEASE LIMITATION
Approved for public release.

UNCLASSIFIED

Produced by

Aerospace Division
Defence Science and Technology Group
506 Lorimer St.
Fishermans Bend, Victoria 3207 Australia

Telephone: 1300 333 362

April 2018
AR-017-017

Conditions of Release and Disposal

Methods of Designing and Feeding Carbon Fibre Reinforced Plastic Slotted Waveguide Antenna Arrays

Executive Summary

This report describes the ongoing development of the Slotted Waveguide Antenna Stiffened Structure (SWASS) technology during the period 2010 to 2012. In SWASS, blade stiffeners in sandwich panels or top-hat stiffeners on skins serve the dual purpose of providing both structural reinforcement while acting as radiofrequency (RF) waveguides. Slots cut through the outer skin and into the waveguides produce slotted waveguide antenna (SWA) arrays. These slots will eventually be filled with a RF transparent dielectric to restore the aerodynamic surface and prevent environmental ingress.

The first half of this report describes the development of a RF design methodology for resonant SWA arrays. The methodology uses an infinite ground plane Finite Element Method model of the SWA. The slot dimensions and location were varied iteratively until the imaginary part of admittance was zero. In this condition the slot resonated because impedance was purely resistive. This approach was validated by correlating its predictions with published data. The validated model was used to design seven- and ten-slot SWA arrays, with longitudinal slots in the broad-wall, for waveguide wall thicknesses the same as that of standard aluminium alloy waveguides, and typical aerospace grade carbon fibre reinforced plastic (CFRP) laminates. Selected designs were manufactured and antenna behaviour measured. The return loss, bandwidth and antenna pattern shape for each array with the same number of slots were similar, regardless of the waveguide material. However the gain of the CFRP antenna was much lower compared to the aluminium alloy equivalent because of significant Ohmic and dielectric losses in the CFRP. Increasing the gain of CFRP SWA would require the conductivity of the inner wall of the waveguide to be increased, which is expected to be straightforward to achieve but would be associated with increased production and through-life-support costs.

The second half of this report describes the development of a plug-and-loop RF feed that; allowed adjacent SWASS waveguides to be fed, had sufficient bandwidth for resonant SWA arrays, and required no electrical connection with, or mounting holes in, the waveguide walls. Plugs were manufactured from aluminium alloy, supported the loop and a coaxial connector, and contained an integral low-high impedance choke. They fitted snugly into the end of CFRP waveguides and were bonded in-place with a structural adhesive. The loops were manufactured from brass shim and soldered to the coaxial connector. The effect of loop dimension on RF performance was measured. These feeds had a bandwidth of 10 % and loss of 0.10 to 0.15 dB, which is considered acceptable for a first generation SWASS demonstrator.

In future the plug-and-loop RF feed will be replaced with one manufactured from CFRP. The new feed could then be incorporated into a SWASS planar array that had been designed using the methodology presented in this report.

This page is intentionally blank.

Authors

Derek Gray
School of Electrical and Computer Engineering – RMIT University

Dr. Derek Gray graduated from University of Manitoba in 2001, having studied novel ehf-band quasi-planar array antennas for terrestrial point-to-point wireless "cable" service. While at Toyota Chuo Kenkyu-jo, he was a junior member of the DTV Team preparing and installing antennas on passenger vehicles, and conducting road trials and demonstrations. Additionally, he worked on prototype injection moulded ceramic antennas for SDARS, VICS, DSRC and ETC. In 2005, he moved to Jouhou Tsuushin Kenkyu Kikou where he initially worked on fault finding for the DTV broadcast trial from a UAV airship and the integration of a DOA into a solar powered stratospheric aircraft wing. The latter culminated in a trial using the Global Observer Prototype, the world's first hydrogen powered aircraft, in 2007. Dr. Gray then worked on equivalent systems onboard a manned airship for post-disaster recovery, an in-cabin WPAN propagation study for the MRJ, developed ehf-band lenses for airliner-to-ground high speed communications, and performed an initial engineering study for a half-metre diameter, 40dBic-class lens for land-mobile/aero-mobile with the Kizune satellite. He was a Research Fellow at RMIT University for the work reported in this paper and now an Assistant Professor at the Department of Electrical and Electronic Engineering, University of Nottingham, Malaysia Campus.

Kelvin J. Nicholson
Aerospace Division

Dr Kelvin J. Nicholson completed his B.Sc in Physics and B.Eng (Hons.) in Electrical Engineering from the University of Melbourne in 2005. He joined the Defence Science and Technology (DST) in 2006 as part of the Aerospace Composites Technology group within the Aerospace Division. As part of this group, Kelvin has been involved in the development of microwave Doppler tomography imaging techniques for the assessment of damaged and repaired composite structures. He has assisted with the mitigation of electromagnetic interference issues aboard the ANZAC frigates and was awarded a Chief Defence Scientist Commendation in 2011 and a Royal Australian Navy Commendation in 2012. Kelvin completed his PhD in Electrical Engineering from RMIT University in 2014 with the support of the DST Enabling Research Program. His current research interests at DST include metamaterials and advanced composite materials for antenna and radar absorbing applications.

Paul J. Callus
Aerospace Division

Dr. Paul Callus has a Bachelor of Applied Science in Metallurgy (South Australian Institute of Technology, 1986) and PhD in Materials Engineering (Monash University, 1993). Since his PhD he has worked with CSIRO developing electrode coatings for ceramic fuel cells then at RMIT investigating the mechanical behaviour of textile composites. He joined Defence Science and Technology Group in 1997 and is currently a Senior Research Scientist in the Advanced Composite Technologies group. His major work programs have focused on the mechanical behaviour of advanced fibre composites, composite replacement panels, airworthiness certification and multifunctional aircraft structure. In 2006/2007 he worked on the topic of conformal load-bearing antenna structure at the Advanced Structural Concepts Branch of the Air Force Research Laboratory at Wright Patterson Air Force Base, Dayton, Ohio.

Kamran Ghorbani
RMIT University

Dr. Kamran Ghorbani received a Bachelor of Engineering degree in Communication and Electronic Engineering (First Class Honours) and PhD degree in Communication Engineering (Antennas and Phase Shifters) both from RMIT University, Melbourne, Australia, in 1995 and 2001 respectively. After his undergraduate degree he worked as an radiofrequency designer for AWA Defence Industries for two years. He joined the RF and photonic research group at RMIT University in 1996 where he pursued his PhD studies. He worked for a telecommunication company (Tele_IP) as a Senior RF engineer mainly working on RF circuit and system design from 1999 to 2001. He joined RMIT University in 2001 and for the last 9 years the focus of his research has been in the areas of broadband and printed antennas, tuneable RF devices, and microwave devices and systems.

Contents

This page is intentionally blank.

1. Introduction

1.1. Conformal Load-bearing Antenna Structure (CLAS)

Conformal Load-bearing Antenna Structure (CLAS) are components or parts that both support structural loads and contain integrated radiofrequency (RF) transmitters and receivers. The term CLAS typically refers to the exterior skin of aircraft manufactured from carbon fibre reinforced plastic (CFRP) [1] however this concept is equally applicable to the exterior skin of civilian vehicles or military platforms used in land, sea or air applications manufactured from other construction material.

The motivation to adopt CLAS is to enhance:

- platform performance (speed, range, endurance and payload) by eliminating the drag and weight associated with conventional externally mounted antennas, particularly blades and wires that protrude from the outer mould line (OML);
- RF performance through;
    - larger antenna radiators or arrays, or
    - conforming to the platform OML.

The platform performance benefits arising from reduced drag are straightforward to conceptualise. Additional explanation is warranted with regard to weight. The traditional approach to installing aircraft antennas is structurally inefficient. Antenna mountings tend to be relatively large so the antennas can retain their dimensions and orientation while being subjected to flight and thermal loading. In addition the underlying structure may need to be reinforced, again to retain antenna orientation but also to restore structural integrity if parts have been drilled or cut to accommodate the mounting. CLAS avoids this inefficiency because antenna support is considered at the design stage, reducing the amount of redundant structure.

The RF performance of traditional antennas is often a compromise between platform performance, which favours small and lightweight antennas, and RF system performance, which often favours large areas or volumes. Conformal antennas may be distributed across more of the platform skin than their conventional blade or wire counterparts thus the individual radiating elements and arrays may be substantially larger. Larger radiators operate at lower frequencies while larger arrays have narrower beams with higher gain.

The combination of enhanced platform and RF performance means that CLAS has the potential to enhance profoundly the capability of military platforms. Platforms could carry systems and perform missions that previously would require vehicles of much larger size.

The CLAS concept was first reported in the early 1990's and since then it has been an active area of research. The largest reported CLAS programs are being sponsored by the United States Air Force (USAF) through the Air Force Research Laboratory (AFRL). The application of CLAS for Australian Defence Force (ADF) has been reviewed elsewhere [1].

1.2. Slotted Waveguide Antenna Stiffened Structure (SWASS)

Slotted Waveguide Antenna Stiffened Structure (SWASS) is a CLAS concept devised by a joint Defence Science and Technology Organisation (DSTO) and AFRL team [2]. In SWASS, the top-hat cross-section stiffeners that are commonly used to reinforce thin aircraft skins, or blade stiffeners in sandwich panels, serve the dual purpose of acting as structural stiffeners and as RF waveguides. Slots are cut through the outer skin, into the stiffener cavities in order to create slotted waveguide antenna (SWA) arrays and the slots are filled with an RF transparent cover to maintain an aerodynamic surface and prevent environmental ingress. Figure 1-1 shows schematics of a conventional sandwich panel and a possible SWASS replacement for that panel.

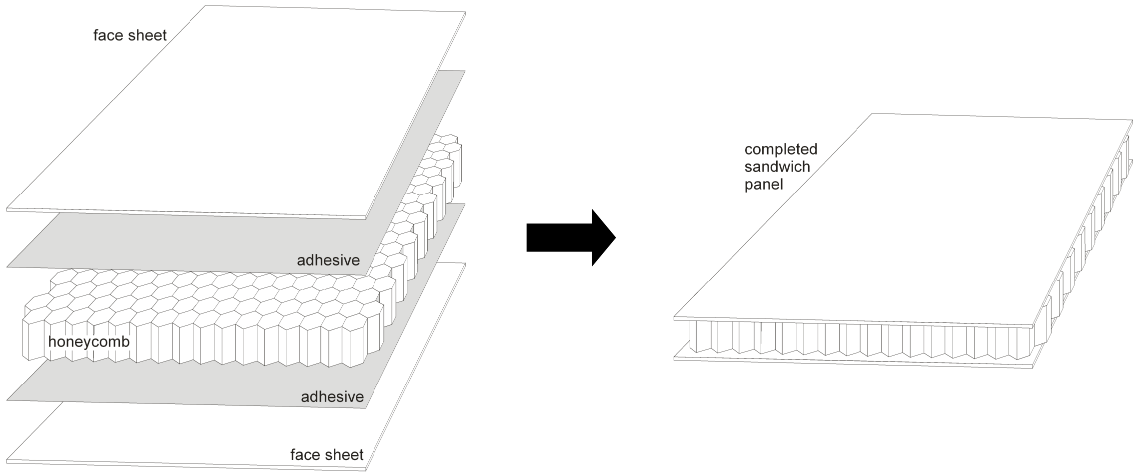

(a)

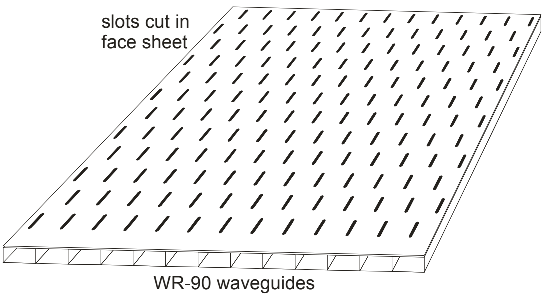

(b)

Figure 1-1 Schematics showing the (a) construction of a conventional honeycomb stiffened sandwich panel and (b) structurally equivalent SWASS panel, a blade stiffened sandwich with waveguide narrow-walls forming the blades and longitudinal slots in the broad-walls

The SWASS concept is being validated and developed through a collaborative program between DSTO and AFRL [2]. The aim of the program is to analyse, design, manufacture and test a demonstrator SWASS panel that operates in the X-band (8-12 GHz), thereby allowing the RF performance to be measured in relatively small anechoic chambers (4-5 m). The demonstrator is to contain waveguide stiffeners that are representative of the size of stiffeners used in structural aircraft panels and which can be manufactured and mechanically tested using existing laboratory scale equipment.

In [2] it was decided that the dimensions of the SWA in the Demonstrator SWASS Panel would match that of WR-90 rigid rectangular waveguides, with an internal cross-section of 22.86 mm x 10.16 mm and operating frequency of 8.2 – 12.4 GHz.

Previous SWASS development work has demonstrated that:

- RF waves can be transmitted through waveguides manufactured from commercially available aerospace grade CFRP with losses that are acceptable, although high, for the Demonstrator SWASS Panel [2, 3], and
- the antenna patterns from single slots in waveguides manufactured from CFRP are similar in shape, but lower gain, to those from the same slot geometry in waveguides manufactured from copper [4].

The studies described in this report extend the previous work by;

- designing, manufacturing, testing and correlating the performance of multi-slot SWA arrays, and
- developing a RF feed for SWASS SWA waveguides that satisfy the dimensional and electrical constraints in a demonstrator SWASS Panel. In particular the feeding method must;
    - allow adjacent waveguides to be fed,
    - be acceptably simple and robust to manufacture and install, and
    - not require intimate physical or electrical contact with the waveguide walls.

1.3. Slotted waveguide antennas (SWA)

Slotted waveguide antennas (SWA) were invented in the 1940s [5, 6]. They are still used today where the application demands structural rigidity, relatively low profile, high power handling capability and very narrow bandwidth.

A rectangular waveguide is a length of electrically conducting tube with internal dimensions such that RF waves of particular frequencies will propagate along that tube. The electric and magnetic fields of waves transmitted along waveguides have characteristic shapes that are known as propagating modes. The guided wavelength (λ_g) in the waveguide is longer compared to the free space wavelength (λ_0) of the same frequency. In most applications, only the fundamental transverse electric propagation mode (TE_{10}) is desired because this transmits energy with minimum loss. A tube will not act as a waveguide if its cross-sectional area is too small as the TE_{10} mode cannot propagate, or if too large will operate inefficiently because higher modes increase propagation loss.

A representation of the instantaneous electrical field (**E**-field) of the TE_{10} mode propagating in a rectangular waveguide is shown in Figure 1-2. The field is oriented parallel to the narrow-walls, the z-direction in Figure 1-2. The field strength profile is sinusoidal across the width (zero field strength at the sidewalls and maximum along the centreline) and along the length (sinusoidal waves oriented in the +z and –z directions) of the waveguide.

The time averaged **E**-field along the waveguide will vary depending on whether the wave is "travelling" or "standing". If the waveguide is terminated with a matched electrical load then a travelling wave will be supported. The wave will propagate down the waveguide(x-direction in Figure 1-2) and be absorbed by the matched load. There will be no reflected wave. The instantaneous wave will have the same sinusoidal pattern along the waveguide, with peaks and nulls at $\lambda_g/2$ intervals, as the incident wave. These peaks and nulls sweep down the waveguide at the phase velocity (υ_p).

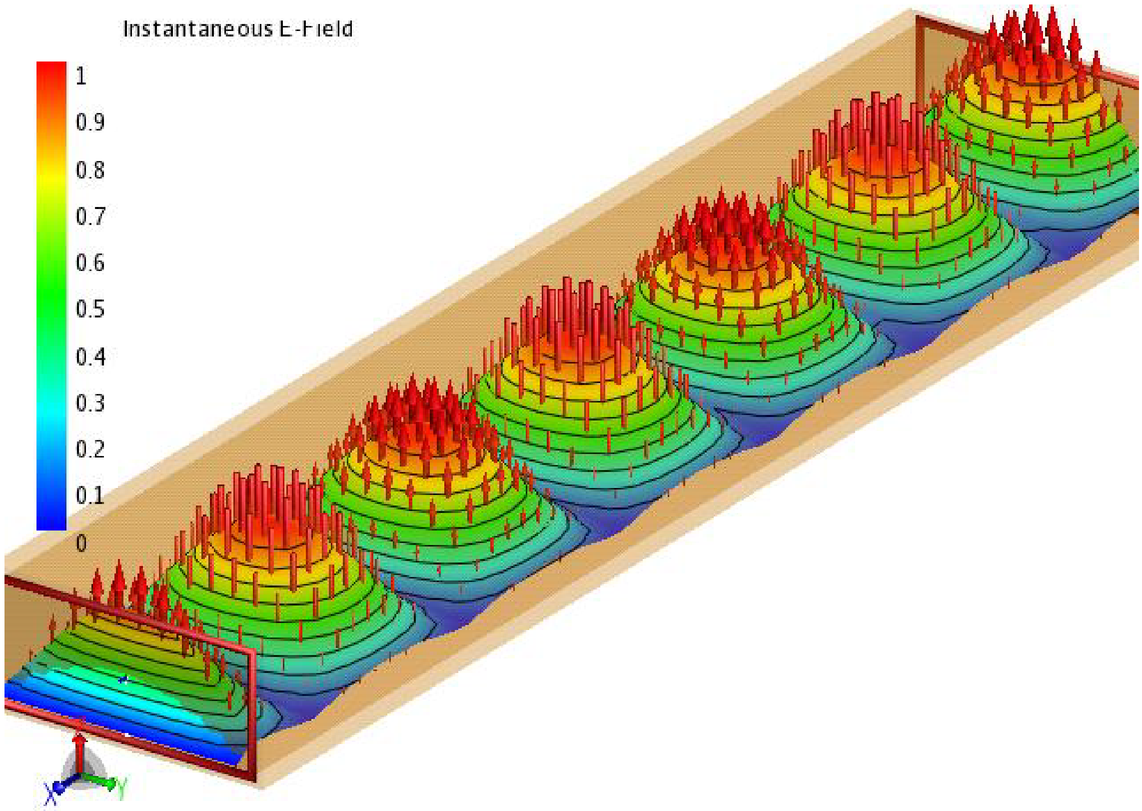

Figure 1-2 Three dimensional representation of the instantaneous E-field in the z-direction, in a rigid rectangular waveguide

If the waveguide is terminated by an unmatched load there will be a reflection back along the waveguide which will add constructively and destructively with the incident wave to create a standing wave. This will be identical shape to that shown in Figure 1-2 but the amplitude of the field will be approximately doubled. The ideal, and most easily realised, non-matched termination is a short circuit, which is conventionally formed by a solid metal plate soldered across the end of the waveguide. Such a plate is a perfect reflecting load because no RF energy can pass through it. Consequently, all of the RF energy input into a short circuit terminated waveguide is retained within the waveguide. The standing wave has a sinusoidal pattern along the length of the waveguide, with peaks and nulls at intervals of half a guided wavelength ($\lambda_g/2$).

The instantaneous electrical currents induced on the waveguide walls by the TE_{10} mode were modelled and are illustrated in Figure 1-3. The two major components of current are;

- longitudinal along the centreline of the broad-wall, and
- circumferential around the narrow-wall. The peaks in the circumferential currents (narrow-wall) are at the same location along the waveguide as the nulls of the longitudinal currents (broad-wall).

It is important to note that the proportions of these changes with frequency. At low frequencies the circumferential narrow-wall currents dominate, while at high frequencies the longitudinal broad-wall currents dominate.

Cutting slots in a short circuit terminated waveguide will create a standing wave resonant SWA, while cutting slots in a matched load terminated waveguide will create a travelling wave SWA. Travelling wave SWA are not considered in this report but may be the focus of future SWASS developments because they offer the potential for broadband antennas.

A resonant SWA consists of a slotted section of standard rectangular waveguide that is terminated with a short circuit. The slots interrupt the currents flowing in the waveguide walls. This creates an electrical field across the slot aperture which radiates into free space. Slots are typically positioned at the peaks of the standing wave in order to maximise the fields. Consequently, SWA are 1-dimensional high-Q resonant cavities. The reliance on a 1-dimensional cavity severely limits both the return loss and radiation pattern bandwidth. These cannot be improved with the use of non-resonant or wideband slots [7].

Despite this electrical limitation, the advantages of high power handling capability and physical simplicity and robustness ensure the popularity of SWA for applications as diverse as small boat maritime radar to space based geo-sensing synthetic aperture radar (SAR). Aluminium alloy is the most common material used for the manufacture of single stick SWA arrays however it is unsuitable for large scale applications because its specific stiffness is insufficient to counter its relatively high coefficient of thermal expansion. Lightweight aluminium alloy arrays distort under thermal or mechanical loads while dimensionally stable arrays are relatively heavy. Consequently, large SWA arrays are often manufactured from composite materials such as polyamide reinforced plastic and carbon fibre reinforced plastic (CFRP). SWA manufactured from CFRP have been used in military maritime radar [8] and space based SAR [9] systems.

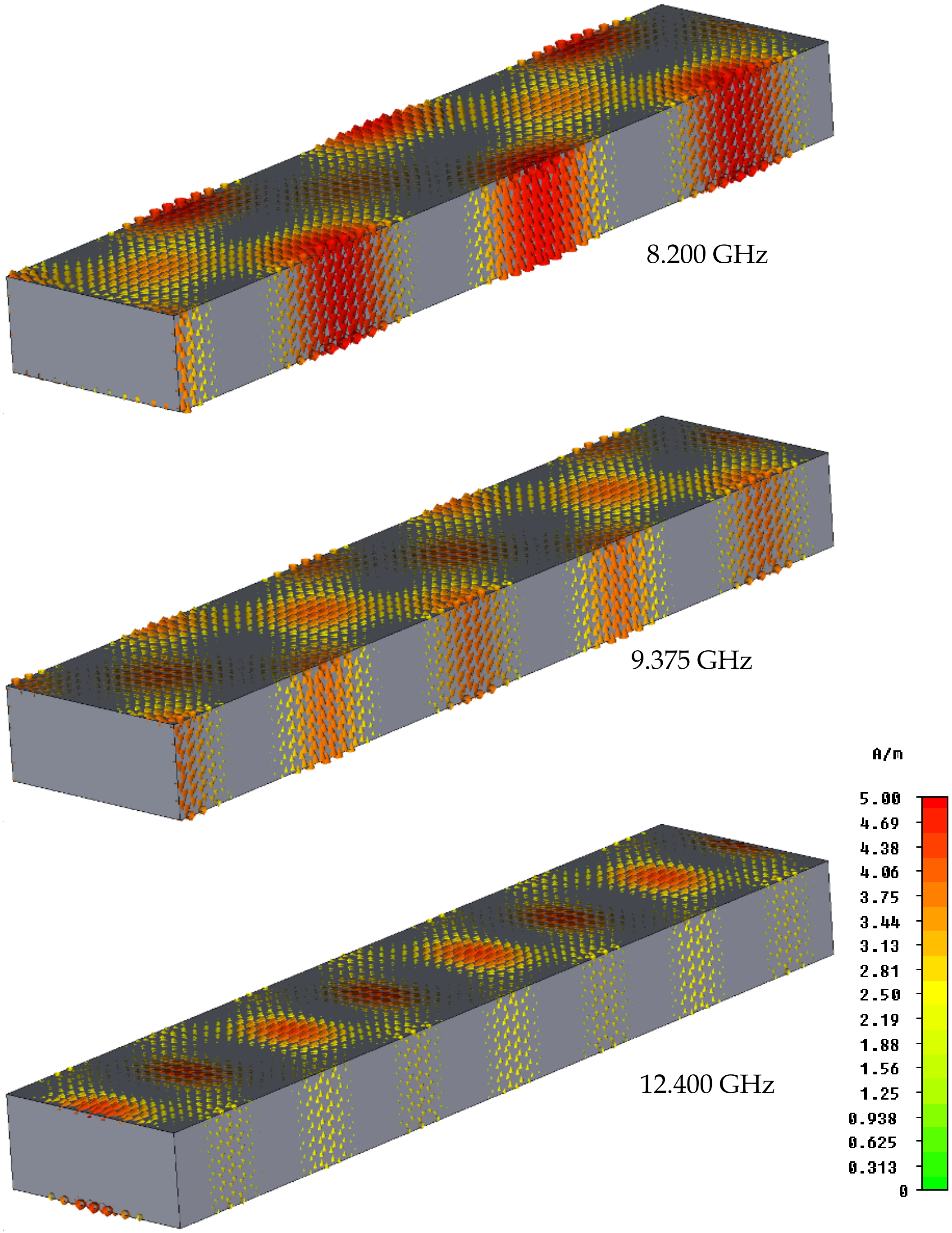

Figure 1-3 Current distribution on the inside of the walls of a section of WR-90 waveguide across the X-band, simulated using the finite-element method for a 1 W source. The primary currents are longitudinal on the broad-wall centreline and circumferential around the narrow-wall but the proportion of these changes with frequency

1.4. Carbon fibre reinforced plastic (CFRP) SWA arrays

SWA arrays have been manufactured from CFRP since the 1980s. They have tended to be used in applications where weight and structural stiffness are critical and costs are secondary, such as space based antennas.

The electrical conductivity of CFRP is substantially lower than that of metals and so the losses in CFRP waveguides are correspondingly higher. Historically these high losses have been mitigated by applying a high conductivity metallic lining to the inside of the waveguide. Approaches have included wrapping the CFRP waveguide material around a metallised dissolvable mandrel [10], adding a metal foil layer around the mandrel [11], using acid erosion to expose the carbon fibres on the inner wall then electro-depositing [12] or sputtering [9] metal onto them.

Although straightforward and effective, lining the inside wall of CFRP waveguides adds complexity and cost to production. In addition, lined waveguides are vulnerable to damage and repair techniques must be capable of restoring electrical conductivity in addition to structural integrity. Thus it is expected that through-life-support costs for lined waveguides would be higher than that of un-lined waveguides. For these reasons one of the aims of the SWASS program is to, wherever possible, use the same materials and processes as employed in the manufacture of standard aerospace components. Therefore methods of minimising the insertion loss when feeding unlined CFRP waveguides were investigated. High conductivity linings are an option for future SWASS components, but would be used if analysis shows that the enhanced antenna performance outweighs the added production and through-life-support costs.

The most common SWA configuration is the longitudinal slot in the broad-wall and this was selected as the configuration for this work. In well-designed structural components the stiffeners are oriented parallel to the major structural loads. Coincidentally, the longitudinal slot is expected to give the least reduction in mechanical performance of a waveguide stiffener subjected to this loading configuration. This is a rare coincidence, the slot geometry that is expected to give good RF performance is also expected to have the least adverse impact on structural performance.

1.5. Introduction to CFRP waveguide feeds

The WR-90 rectangular waveguide is the preferred transmission line for high power application in X-band. It is both physically robust and electrically sealed. However rectangular waveguides cannot connect directly to common testing equipment such as the Vector Network Analyser (VNA). Thus there is a need for an adaptor between coaxial cables and the waveguide, a so-called coax-to-waveguide adaptor.

The most common coax-to-waveguide adaptor is a probe fed through a small circular hole in the broad-wall of the waveguide [15-17] as pictured in Figure 1-4. The vast majority of commercially available WR-90 coax-to-waveguide adaptors are of this configuration. The probe extending into the waveguide is usually of greater diameter compared to the coaxial connector pin and is often surrounded by a cylinder of cross-linked polystyrene in order to broaden the matching bandwidth. Furthermore, a short grub screw in the opposite wall is often used to fine tune the adapter for optimum performance over the waveguide band. Regardless of the exact probe design, a short circuiting plate is positioned at a distance of $\lambda_g/8$ of the centre frequency behind the probe. It is possible that this concept may be used in a device to feed SWASS waveguides however, a practicable and manufacturable design that allowed adjacent waveguides to be fed was not sought.

For the CFRP waveguides used in SWASS parts the coax-to-waveguide adapter must be able to function without requiring intimate physical or electrical connection with the waveguide walls because achieving a “perfect” joint is impracticable. In “as-manufactured” CFRP laminates, the high conductivity carbon fibres are covered with a layer of polymer resin that is in the order of a few microns to tens of microns thick. Abrading sufficient resin to expose the top layer of fibres may facilitate good connection with these fibres, but the deeper fibres will not be connected directly. Abrading further into the laminate will allow the deeper fibres to be connected but will degrade structural performance. This is particularly harmful for fibre composites because in most load cases the fibres support the majority of the load (over 90 % in some cases).

An alternative concept which offers superior bandwidth performance to the probe method is the antipodal fin line waveguide-to-microstrip transition [18] pictured in Figure 1-5. This is commonly used to integrate phase shifters, amplifiers and filters into waveguides. In it, a printed circuit board is located between the centres of the broad-walls and oriented in the waveguide longitudinal direction. Antipodal fins are printed on either side of the board. The long thin fin (right hand end in Figure 1-5) is soldered to the centre pin of the coaxial feed while the antipodal fin on the other side is flared to provide a ground plane.

This type of transition was judged unsuitable for SWASS for two reasons. Firstly, a minimum taper length of $2\lambda_g$ (preferably $3\lambda_g$) is needed. This equates to approximately 120 mm at 10 GHz, which is impractical if the SWASS components were only a few hundred mm long, which is expected to be the case for the Demonstrator SWASS Panel, or where structural considerations demand that the ends of the waveguide stiffeners be relatively close to the edge of the component. Secondly, the ability of the tapered transition to couple all the available power into the microstrip line is dependent upon suppression of the TE_{10} mode. Failure of the slotted line and microstrip ground plane to make perfect electrical connection with the waveguide walls would mean incomplete suppression of the TE_{10} mode. Again, it was considered impractical for this to be achieved in a SWASS component.

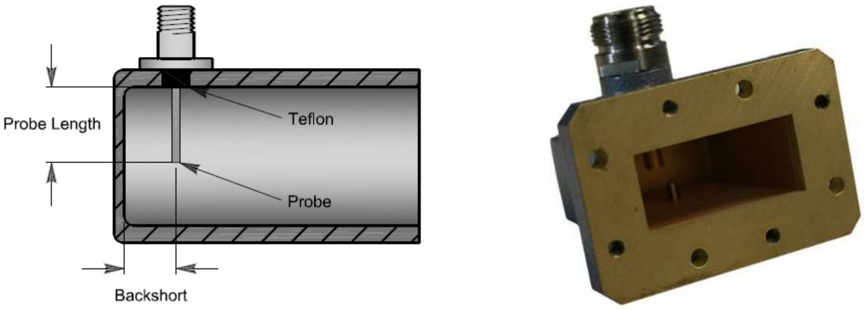

(a) (b)

Figure 1-4 A (a) drawing showing the critical dimensions [33], and (b) photograph of a typical commercially available coax-to-waveguide transition

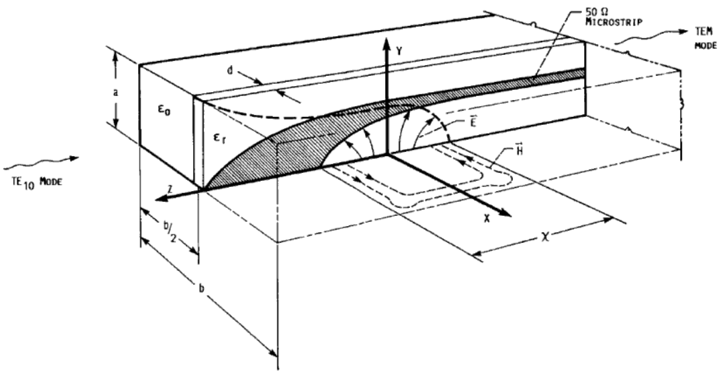

Figure 1-5 Diagram of a tapered slot transition [18]

A less common type of commercially available coax-to-waveguide transition consists of an extension of the coaxial centre pin through a short circuit end plate. The centre pin connects to a four stepped section that is welded or bolted to the centre of one broad-wall [19]. A known variation of this type of end feed has a small dielectric isolating block between the end of the stepped section and the waveguide wall as pictured in Figure 1-6.

This concept appears applicable to SWASS waveguides. The metal stepped section is not required to make direct physical contact with the waveguide wall, which is required for a CFRP waveguide. The as-manufactured layer of epoxy encapsulating the fibres may then be left untreated. For example, a sub-miniature version A (SMA) coaxial connector may be fastened to a backing plate that contains a central hole through which the centre conductor may be soldered to a stepped section manufactured from brass shim. The backing plate would be bonded into the end of the CFRP waveguide. The main impediment to this type of feed is the requirement to optimise the height and length of the four steps in the loop. Such an optimisation involving ten variables could be undertaken by a suitable software package however it was expected to be time-consuming and was not pursued in this work.

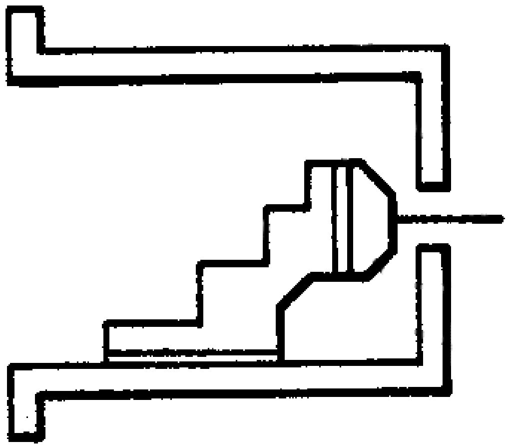

Figure 1-6 Diagram of the cross-section of a stepped transition with dielectric spacer [20]

A simpler, albeit narrow band, version of an end fed stepped transition is a simple wire loop [21, 22] as illustrated in Figure 1-7. Simple wire loops constructed using the coaxial connector centre pin, bent at 90° and terminated at the centre of the broad-wall, have been studied and are well understood [21]. Obtaining the desired frequency requires only the length of the loop to be chosen correctly, which is one variable compared to the ten required for the four stepped concept described in the previous paragraph.

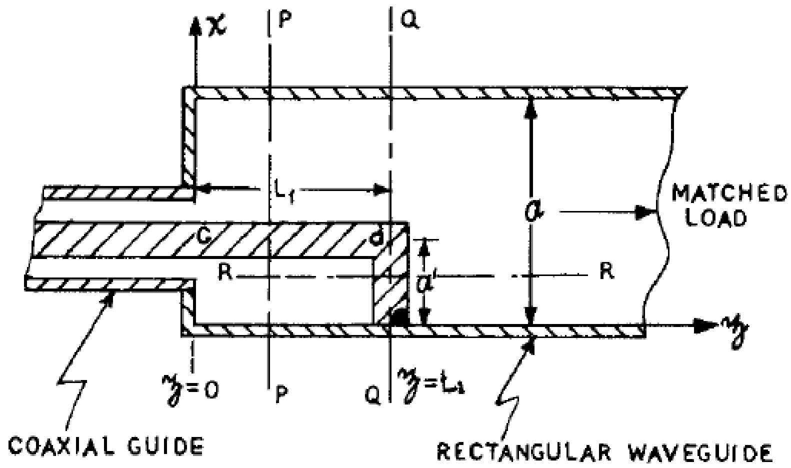

Figure 1-7 Diagram of the cross-section of a wire loop end feed [21]

The published designs for the simple wire loop end feed have the wire loop terminating on the broad-wall. This was not possible for the CFRP waveguides in SWASS and so a suitable alternative was sought. The selected solution was the plug-and-loop design shown in Figure 1-8. The loop was replaced with folded brass shim with one end soldered to the centre conductor of a SMA connector (Sub-miniature Type A Female Flange, SMA/F Flange) connector and the other to the outer braid of the SMA connector. The loop and SMA connector were mounted onto an aluminium alloy plug that could be slid into the end of CFRP waveguides. The plug also contained an integral low-high impedance choke in order to minimise RF leakage through the gap between the waveguide wall and plug.

An advantage of the plug-and-loop feed is that the dimensions of the brass shim loop may be adjusted to give the widest possible bandwidth with minimal losses at the design frequency. The effect of brass shim width and loop length on RF loss is detailed in Section3 of this report.

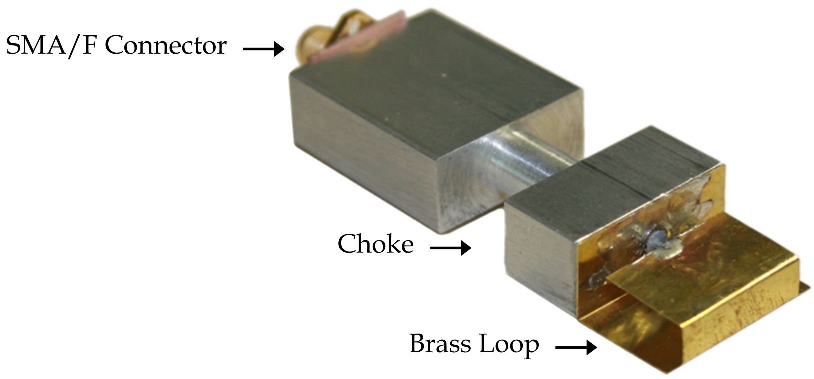

Figure 1-8 A prototype plug-and-loop RF feed for CFRP waveguides

2. Radiofrequency Design of SWA Arrays

2.1. Aim

Section 2 details the development and validation of the RF design methodology for resonant SWA arrays. This validated RF design methodology may be used to design either single stick or planar resonant SWA arrays, with uniform or non-uniform aperture distribution, manufactured from metal or CFRP. In this work, the methodology was used to design single stick SWA arrays with a uniform amplitude aperture distribution. Slot resonant length depends on wall thickness [13, 14]. Since both aluminium alloy and CFRP waveguides are to be designed in this work, and their thicknesses are different, then different slot lengths were required.

The authors were unable to identify any literature that clearly described a RF design process that produced a working resonant SWA array. Hence Section 2 details the design methodology and will therefore serve as a reference for future work on SWASS.

In this work it was decided to produce single stick SWA arrays with longitudinal slots in the broad-wall, because:

- this slot orientation is expected to be structurally efficient,
- RF simulations may be compared with those in the literature, and
- single stick, multi-slot, SWA arrays represent the next-level of manufacture and test complexity from the single-slot SWA evaluated previously in the SWASS program [3].

2.2. Design variables for SWA arrays

The design variables for a SWA, as shown in Figure 2-1, are the;

- slot orientation
  - longitudinal or inclined
  - broad-wall or narrow-wall
- number of slots
- slot position
  - slot offset (from waveguide centreline)
  - slot separation
- slot dimensions
  - slot length
  - slot width
  - slot thickness (waveguide wall thickness).

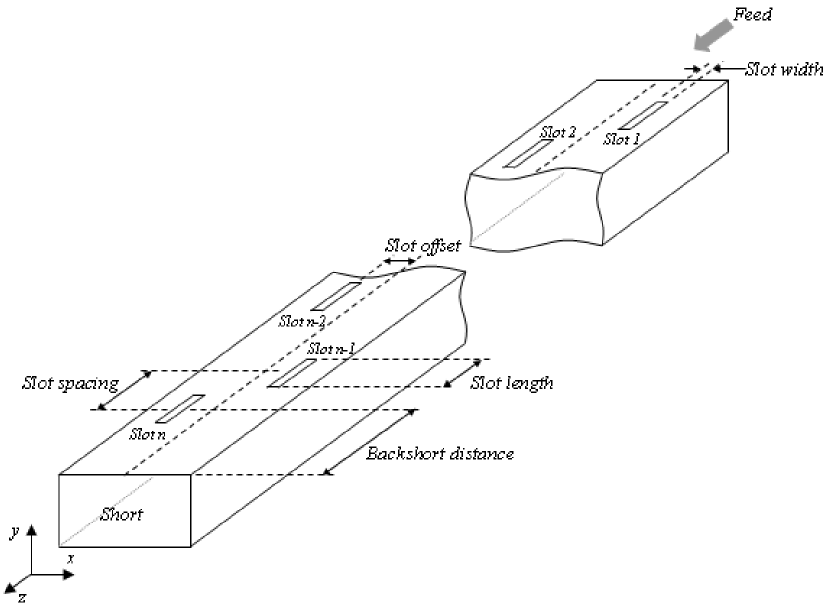

Figure 2-1 Diagram of an n-slot SWA showing the design variables. In this SWA, the radiation pattern would be broad in the E-plane (x-y plane) and narrow in the H-plane (y-z plane)

The slot orientation and number of slots are generally set by the beamwidth and gain requirements. Slot thickness will be equal to the thickness of the waveguide. The design of slot length and offset requires substantial computational effort and experimental validation. The slots are designed to produce the desired power output but with a impedance that matches that of the feed waveguide (radiofrequency matching).

2.3. Numerical model and design procedure for SWA arrays

The key to designing SWA arrays is to establish the resonant slot length. Historically this has been found through laborious and costly trial and error or the use of custom-made Method-Of-Moments software [14, 23]. Modern commercially available software packages such as Electromagnetic Software & Systems-South Africa (Pty) Ltd (EMSS-SA) FEKO [24], Computer Simulation Technology (CST) Microwave Studio® (CST MWS) [25] and Ansys High Frequency Structure Simulator™ (HFSS™) [26] offer the possibility of a more convenient option where the resonant slot length can be found by simulating a short length of waveguide with a single slot [27]. The optimisation process consists of iteratively changing the slot length until the shunt admittance of the short length of waveguide is a pure conductance. This process will be described further in Section 2.5.

It was decided that this part of the RF design methodology for SWASS would be based on the finite-element (FEM) solver in HFSS™. The FEM model consisted of an infinite ground plane with a prism representing the WR-90 rectangular waveguide and a larger prism representing the radiation space. The slots were modelled as round ended blocks that had the height of the waveguide wall and connected the two large prisms. Hence, the FEM approach simulated the air spaces inside the antenna, in contrast to the Method-Of-Moments (MoM) approach which would have simulated the waveguide structures. A 10-slot SWA as implemented in HFSS™ is illustrated in Figure 2-2.

As indicated previously, the open literature does not contain any tutorial type descriptions of the resonant SWA array design process. The papers that provided greatest insight into this process were [23] and [28]. The following four step process was evolved to design resonant SWA arrays using modern commercially available electromagnetic simulation software:

1. Characterise the slot shunt admittance as a function of slot offset and slot length for the specified waveguide wall thickness using the design cell described in Section 2.5. A simple parametric sweep in HFSS™ was used to compile the necessary characterisation curves.
2. Specify the slot offset to give the desired aperture distribution. For this work, a constant slot off-set was used.
3. Select the resonant slot length for the specified slot offset from the characteristic curves in Step 1.
4. Simulate the array performance and refine the back-short distance to obtain the return loss that most satisfies the design requirements; minimal return loss for high power applications or maximum bandwidth if it is necessary to accommodate manufacturing tolerances.

2.4. Validating finite element model

The FEM model was validated by correlating its predictions against experimental results reported in the literature. Unfortunately, there are very few SWA designs published in the open literature that provide (i) all dimensions, (ii) the return loss and (iii) radiation patterns across a range of frequencies.

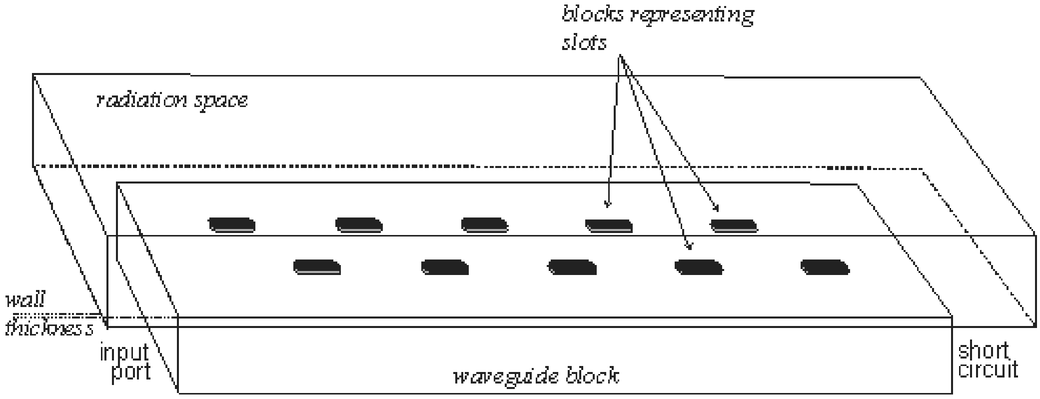

Figure 2-2 Infinite ground plane FEM model of 10-slot slotted waveguide antenna

Reference [28] was found to most closely satisfy these requirements. In that work, a 7-slot resonant SWA array in WR-62 waveguide was designed to operate at 14.03 GHz. This is different to the planned CFRP SWA array in WR-90 waveguide operating at 9.375 GHz. However, the design methodology is scalable and so this difference was considered inconsequential.

The HFSS™ FEM model shown in Figure 2-2 was created with the dimensions specified in [28]. The critical information missing from [28] was the WR-62 waveguide material and wall thickness. It was inferred, on the basis of the date and author affiliation of [28] that the waveguide material was brass and the wall thickness was 1/40" (0.635 mm). Thus the wall thickness in the FEM model was set to 0.635 mm.

The back-short distance specified in Figure 2-1 was denoted d_o in [28]. This dimension is usually set as an odd multiple of $\lambda_g/4$ so that the peak of the standing wave created when the forward (incident) wave constructively interferes with the backward wave (reflected from the short circuit) is centred on the slot. One very interesting aspect of [28] was that d_0 was used to improve the input match. In [28] the return loss for d_o = 19, 20 and 21 mm were calculated. This return loss was also simulated using the FEM model and both sets of results are overlaid in Figure 2-3 (a). The close approximation suggests that the infinite ground plane FEM model was able to simulate adequately the near field and mutual coupling between the slots.

The measured H-plane (y-z plane from Figure 2-1) radiation patterns were shown in Fig. 10 of [28] for five frequencies from 13.0 GHz to 15.25 GHz and are reproduced in Figure 2-3 (b) to (f). The pattern changed from a broad slightly conical beam at lower frequencies, through a well-defined single main lobe at the design frequency and then to a clearly conical beam at the highest frequency. From these figures the useable bandwidth was estimated as 3% to 4%, which is very narrow compared to other low to medium gain antenna types.

Antenna patterns were simulated using the infinite ground plane FEM models at the same frequencies as shown in Fig. 10 of [28] and both sets of results overlaid in Figure 2-3 (b) to (f). There was excellent agreement between the measured and simulated H-plane main beam and side lobe amplitudes and locations at all frequencies except for 13.6 GHz.

At 13.6 GHz, the position of the simulated and measured side-lobes matched well, however the simulated side-lobe level (SLL) was up to 5 dB higher compared to the measured SLL. The FEM simulation was repeated at 13.75 GHz so that the peak of the first side lobe in the negative θ direction matched that of the measured antenna. Although the match for this side lobe was now excellent, the match in position of the remaining side lobes was worse. The discrepancies between simulated and measured H-plane antenna pattern for this frequency remain unexplained.

No comparison was made to the E-plane (y-x plane from Figure 2-1) radiation patterns as these were not published in [28]. The E-plane radiation patterns predicted by the FEM model appear to be as expected, a single broad beam.

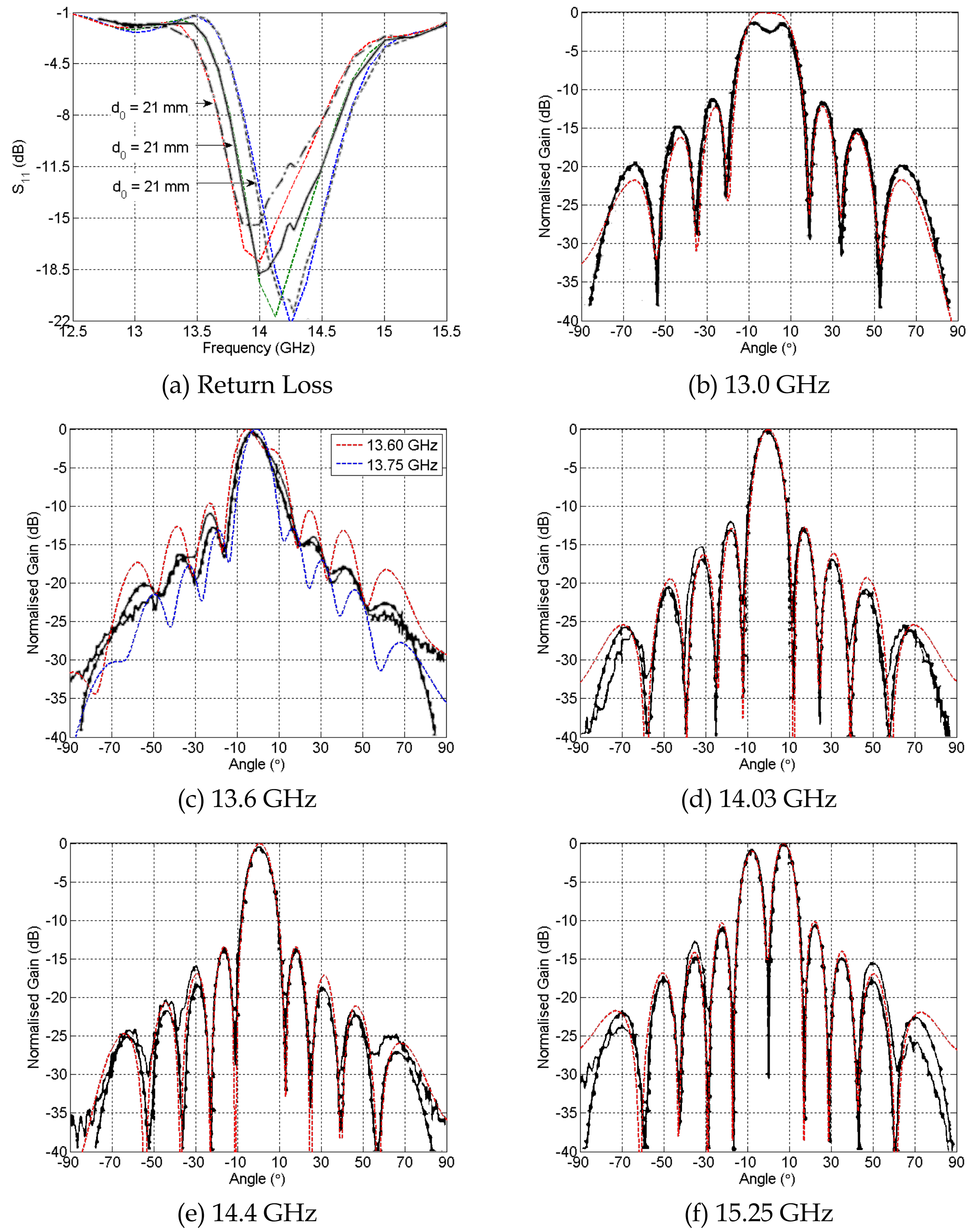

(a) Return Loss

(b) 13.0 GHz

(c) 13.6 GHz

(d) 14.03 GHz

(e) 14.4 GHz

(f) 15.25 GHz

Figure 2-3 *Measured and predicted (a) return loss, and (b) to (f) H-plane antenna patterns for a 7-slot WR-62 SWA array. Measured values are from [28] and appear as the black background to each plot. The smooth coloured curves on each plot are the patterns simulated with an infinite plane FEM model*

The very good agreement between the measurements published in [28] and the FEM simulations, notwithstanding the unexplained differences at 13.6 GHz, verified that the relatively simple infinite ground plane model was capable of simulating accurately the return loss and H-plane radiation patterns of the resonant SWA array.

2.5. Single slot resonant length

The resonant length of a slot for a particular offset from the centre line is dependent upon the frequency and the thickness of the waveguide broad-wall. This makes each resonant slot length and offset unique to the frequency and wall thickness, which in turn are dictated by the antenna specifications and the available materials.

The resonant slot length for a given offset from the centre line, frequency and wall thickness can be found by simulating the single slot in a resonant section of waveguide and tuning the slot length to achieve a purely real admittance in a one port model [27] or maximised radiation efficiency in a two port model [29]. Either method may be fully automated using single variable optimisations in commercially available software. The method from [27] was chosen due to the ease with which the simulation results could be directly compared to the experimental results available in [30].

The FEM single slot design cell illustrated in Figure 2-4 was created in HFSS™. Its construction was identical to the FEM model validated in Section 2.4. However this model consisted of a $3\lambda_g/4$ length of WR-90 waveguide with a single slot rather than the 10-slot array of Figure 2-2. The centre of the slot shown in Figure 2-4 was positioned $\lambda_g/2$ from the input port in order to transform the impedance of the slot to the face of the port, while the terminating short circuit was $\lambda_g/4$ from the centre of the slot. The radiation space was a hemisphere centred on the slot in contrast to the rectangular prism of Figure 2-2. The slot width was fixed at 1.6 mm because this was achievable using the available manufacturing facilities (a computer numerically controlled router with conventional end mills for aluminium alloy or diamond coated tool bits for CFRP). Coincidently, this slot width matched the prior experimental work on single slots [30].

The FEM single slot design cell was used to establish the resonant slot length by varying slot length for a given slot offset from the centreline, until the imaginary component of the shunt admittance equalled zero. At this length the shunt admittance of the slot becomes a pure conductance. This was the same approach as in [27]. A sample result is shown in Figure 2-5 for a wall thickness of 1.27 mm and an offset of 3.0 mm from the centreline. The simulated shunt admittance is a pure conductance when the slot length is 15.8 mm. Using this model the resonant slot lengths for centreline offsets between 1.8 and 4.0 mm and wall thicknesses of 0.50, 1.27 and 3.00 mm were also calculated. These are detailed in Table 2-1 and plotted in Figure 2-6.

The 7- and 10-slot SWA arrays were designed with the data from Table 2-1 using the process detailed in Section 2.3. It is not practicable to manufacture real arrays to the four decimal place accuracy specified in the "Slot length (mm)" columns of Table 2-1, so for the experimental arrays these lengths were rounded to the nearest 0.1 mm. These rounded lengths are shown in the “Slot lengths used in 7- and 10-slot arrays” columns of Table 2-1.

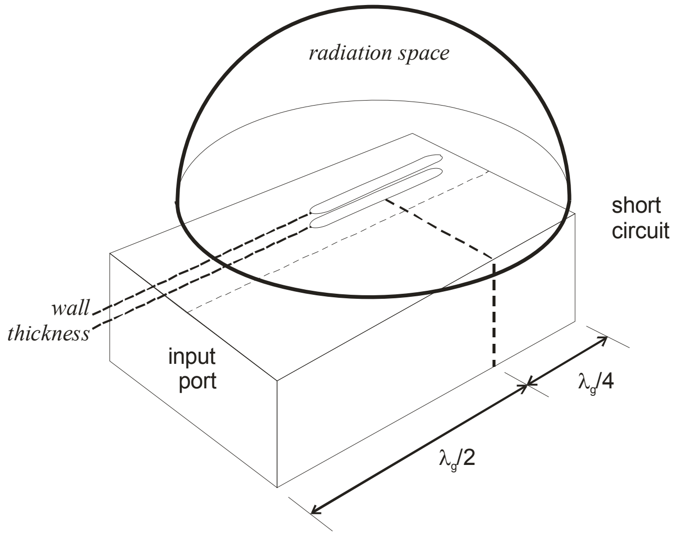

Figure 2-4 FEM single slot design cell, after Brown [27]

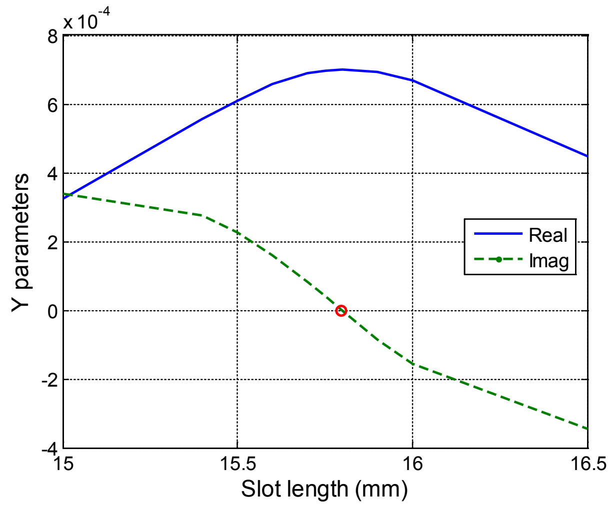

Figure 2-5 The effect of slot length on slot admittance (Y) of a 3.0 mm offset in a WR-90 waveguide with 1.27 mm wall thickness at 9.375 GHz as simulated in the single slot design cell

The simulated resonant slot lengths for each array and wall thickness are plotted in Figure 2-6. These curves were created by considering the equivalent electrical circuit for a slot shown in Figure 2-7 and the definition of admittance shown in Equation 2.1. Maximum power transfer for any given slot configuration (width, offset and wall thickness) will occur when slot length is tuned until the admittance is a pure conductance (i.e. B = 0). At this length the reactance defined in Equation 2.2 becomes zero and the impedance purely resistive.

Table 2-1 Effect of slot centreline offset and wall thickness on slot resonant length at 9.375 GHz as simulated by the single slot design cell FEM model. The data from this table is plotted in Figure 2-6

Slot offset (mm)	**0.50 mm wall thickness**		**1.27 mm wall thickness**		**3.00 mm wall thickness**	
	Slot length (mm)	**Slot lengths used in 7- and 10-slot arrays**	**Slot length (mm)**	**Slot lengths used in 7- and 10-slot arrays**	**Slot length (mm)**	**Slot lengths used in 7- and 10-slot arrays**
1.8	15.3048		15.5921	15.6 mm for 10-slot	15.8765	
1.9	15.3316		[redacted]		15.8936	
2.0	15.3570	15.4 mm for 10-slot	15.6339	15.4 mm for 7- & 10-slot	15.9093	
2.1	15.3810		15.6528		15.9238	
2.2	15.4038	15.4 mm for 10-slot	15.6708		15.9372	
2.3	15.4257		15.6878		15.9497	16.0 mm for 10-slot
2.4	15.4468		15.7042		15.9615	
2.5	15.4673	15.5 mm for 10-slot **Final 10-slot**	15.7200	15.7 mm for 7- & 10-slot **Final 10-slot**	15.9727	16.0 mm for 10-slot
2.6	15.4875		15.7355		15.9834	
2.7	15.5074	15.5 mm for 7- & 10-slot	15.7508	15.75 mm for 10-slot	15.9939	16.0 mm for 10-slot **Final 10-slot**
2.8	15.5273		15.7660	15.8 mm for 10-slot	16.0042	
2.9	15.5473		15.7814		16.0146	
3.0	15.5677		15.7970	15.8 mm for 7- & 10-slot	16.0252	
3.1	15.5887		15.8131		16.0361	
3.2	15.6101	15.6 mm for 7-slot **Final 7-slot**	15.8297		16.0474	16.0 mm for 7-slot **Final 7-slot**
3.3	15.6320		15.8466		16.0589	
3.4	15.6543		15.8640		16.0707	
3.5	15.6770	15.7 mm for 7-slot	15.8816	15.9 mm for 7- & 10-slot **Final 7-slot**	16.0828	16.1 mm for 7-slot
3.6	15.7001		15.8997		16.0951	
3.7	15.7236	15.7 mm for 7-slot	15.9179		16.1076	16.1 mm for 7-slot
3.8	15.7473		15.9365		16.1202	
3.9	15.7714		15.9553		16.1331	
4.0	15.7956		15.9743	16.0 mm for 7- & 10-slot	16.1460	

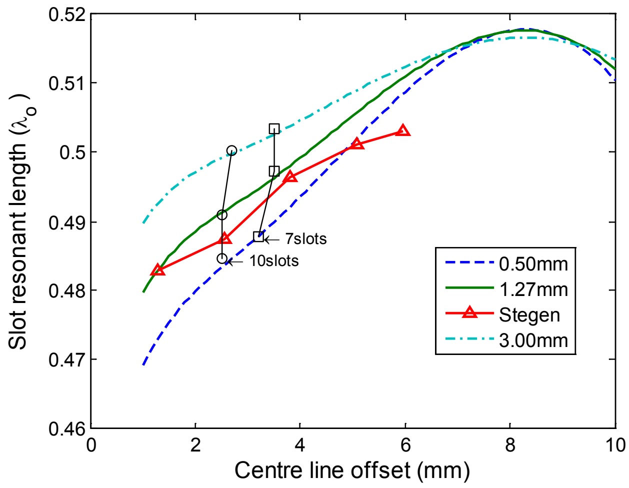

Figure 2-6 The effect of slot centreline offset and wall thickness on slot resonant length at 9.375 GHz as simulated by the single slot design cell FEM model and measured for a 1.27 mm wall thickness by Stegen [30]. The simulated offset and rounded slot length for the designed 7- and 10-slot SWA arrays are also shown

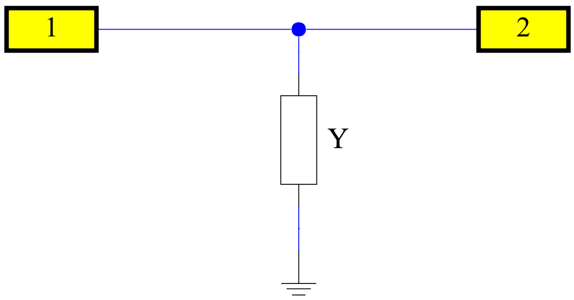

Figure 2-7 The equivalent circuit for a single slot. The waveguide is represented by Ports 1 and 2 while the slot is represented as a shunt admittance (Y) in the transmission line

$$Y = G + jB \tag{2.1}$$

$$Z = Y^{-1} = R + jX \tag{2.2}$$

Where:

j^2 = -1

Y = Admittance (S)

G = Conductance (S)

B = Susceptance (S)

Z = Impedance (Ω)

R = Resistance (Ω)

X = Reactance (Ω)

Figure 2-6 also shows the experimental results from [30]. There was good agreement with the simulation for the same wall thickness (1.27 mm), particularly for offsets less than 5.0 mm. This provided additional confidence in the simulations.

The energy radiated by a single slot is proportional to the conductance of that slot and the input impedance of the total SWA is governed by the sum of the conductance from each of the slots. Multiple SWA configurations, with different slot lengths offsets and wall thicknesses, were developed in this work. Figure 2-8 shows that, despite these differences, for small slot offsets the conductances of the slots do not depend on wall thickness. Thus it is valid to compare directly the performance of SWAs fabricated from aluminium alloy (1.27 mm wall thickness) and CFRP (0.5 mm wall thickness).

2.6. Sample array design

7-slot and 10-slot resonant SWA arrays were designed for 9.375GHz and wall thicknesses of:

0.50 mm	Thickness of a 4-ply CFRP waveguide.
1.27 mm	Thickness of standard commercially available extruded copper, brass and aluminium alloy waveguide.
3.00 mm	Thickness of a typical CFRP aircraft panel.

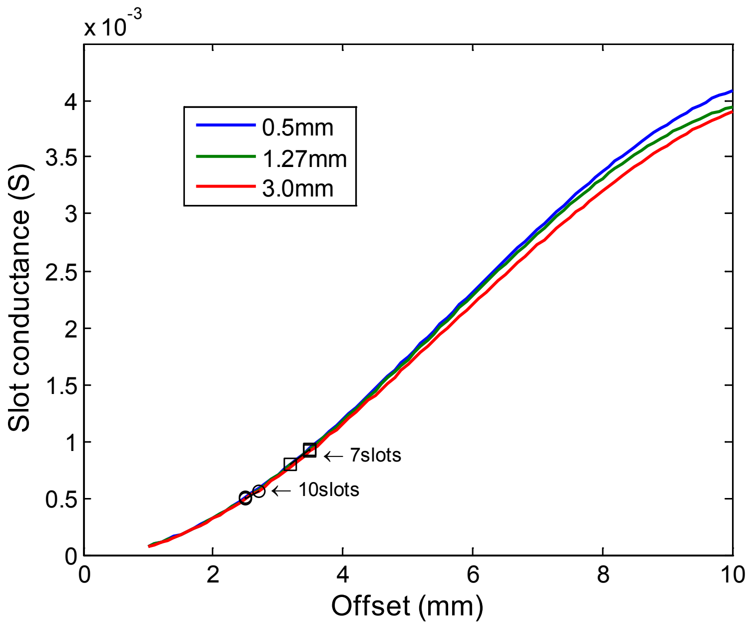

Figure 2-8 Effect of slot offset and wall thickness on slot conductance at 9.375 GHz as derived from the single slot design cell FEM model

It was decided that each of the six resonant SWA arrays designed in this work would have a uniform amplitude taper and hence constant slot length and slot offset from the centre-line, although these lengths and offsets would be different for the 7- and 10-slot arrays to ensure impedance matching. This would simplify the design process but was still expected to provide SWAs with reasonable performance. In [28] it was shown that the performance of the 7-slot array with uniform slot length and offset was reasonable.

It is certainly possible to use different slot lengths and offsets in order to optimise radiation performance and impedance matching [31, 32]. The benefits of these techniques are expected to be significant in antennas manufactured from reduced height waveguides where the inter-slot coupling is high.

An infinite plane FEM model was created for each array design. The return loss of several slot length/offset combinations from Table 2-1 was simulated for each slot number/wall thickness combination. A total of approximately fifty simulations were conducted. The predictions are shown in Figure 2-9, Figure 2-10 and Figure 2-11.

The return loss behaviour for each SWA configuration (number of slots, wall thickness) was predicted to vary with slot length/offset. Behaviour varied from a distinct resonance with a sharp and deep null and a -10 dB band width (frequency range over which return loss was below -10 dB) in the order of 5 % through to a broad trough where return loss dipped moderately over a broader -10 dB bandwidth.

In addition, the bandwidth of the 10-slot SWA arrays was narrower than that of the 7-slot SWA arrays. This may be explained by considering the SWA as a high-Q cavity supporting a simple standing wave. Increasing the cavity length increases its Q values and hence reduces its bandwidth.

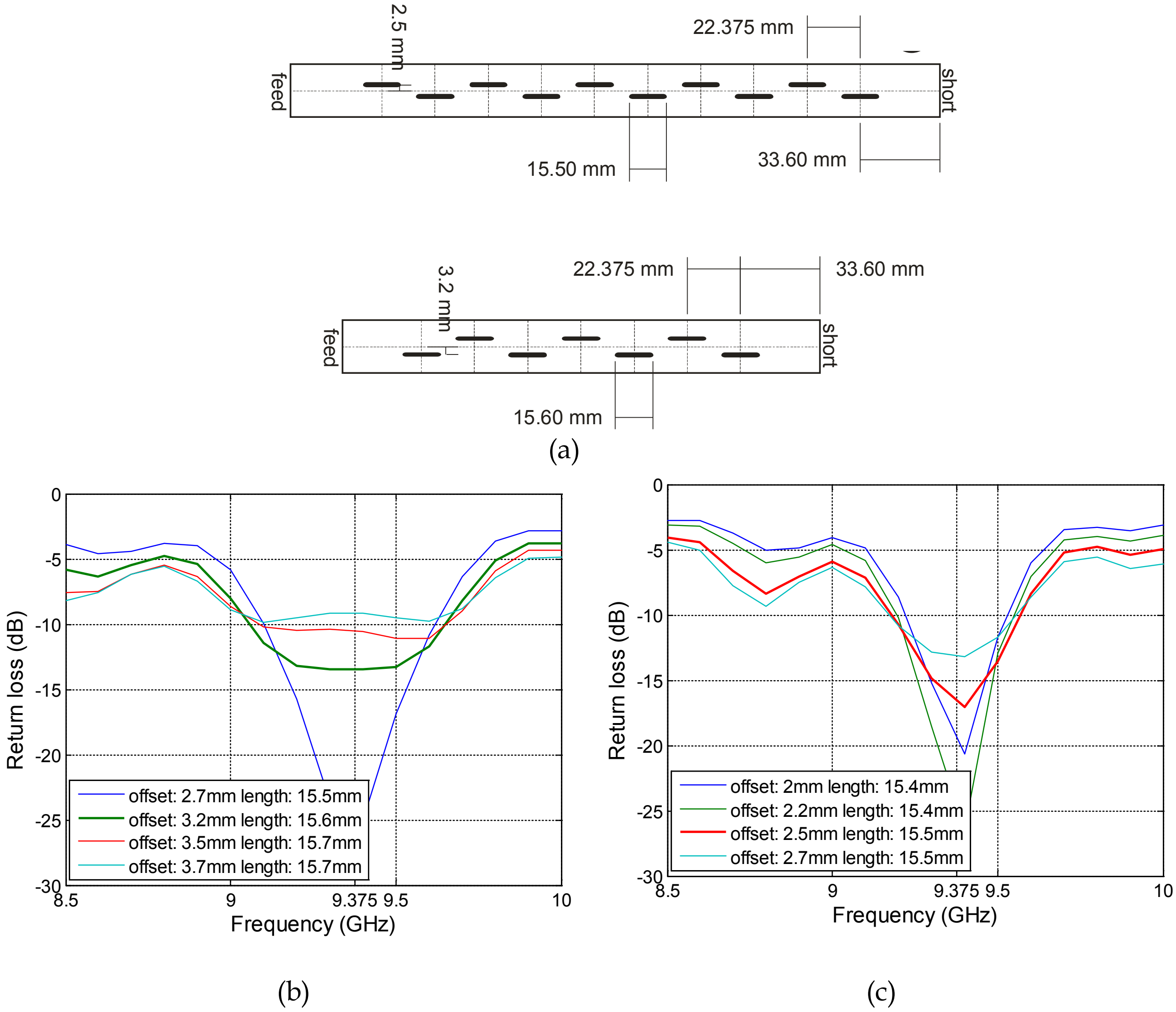

Figure 2-9 *(a) Dimensions and simulated return loss as simulated in the single slot design cell FEM model for (b) 7-slot and (c) 10-slot arrays with 0.50 mm wall thickness (4-ply CFRP)*

For each simulation the return loss from 8.5 to 10.0 GHz was compared and the subjective "best" design selected. The final 7-slot designs were selected on the basis of broader bandwidth because this was inherently larger in the shorter array and the design was more tolerant to manufacturing errors. The 10-slot designs were selected on the basis of improved matching (deeper null at resonance) that would be more suited to high power applications.

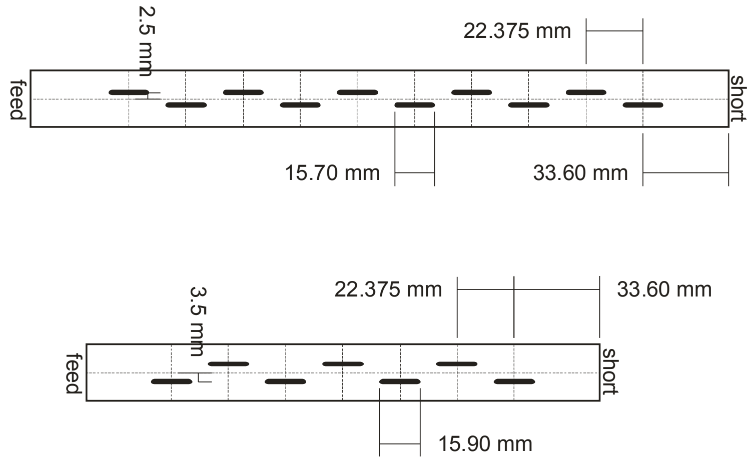

(a)

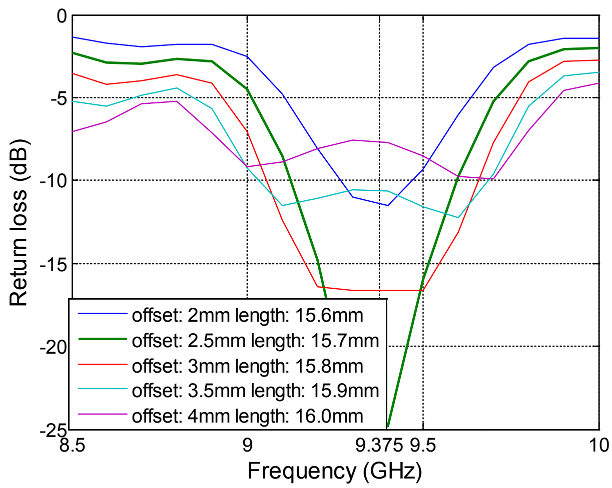

(b)

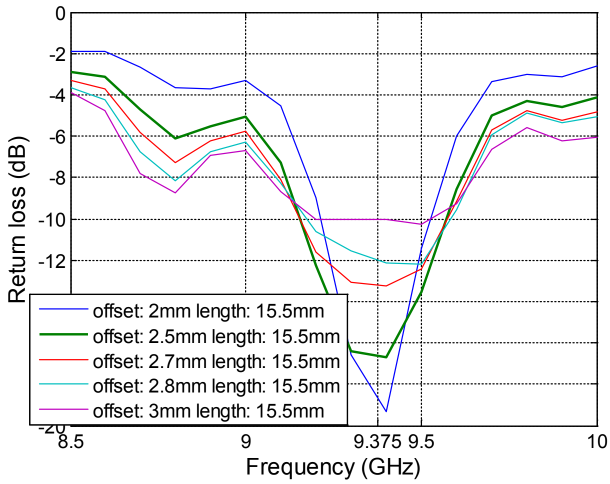

(c)

Figure 2-10 (a) Dimensions and simulated return loss as simulated in the single slot design cell FEM model for (b) 7-slot and (c) 10-slot arrays with 1.27 mm wall thickness (standard WR-90 waveguide)

2.7. Method of Moments simulation of selected array designs

Four of the arrays designed in Section 2 were selected for manufacture and test. These were the 7- and 10- slot arrays manufactured from 0.50 mm thick CFRP (Figure 2-9) and 1.27 mm thick aluminium alloy (Figure 2-10).

In addition to the simulations shown in Section 2, which used simplified FEM models to calculate return loss for design purposes, the behaviour of the 10-slot arrays was also simulated using a full Method-of-Moments (MoM) solution implemented in FEKO™. The FEKO™ MoM software was used because in this case the computer memory requirements were significantly below that required for the HFSS™ FEM solver.

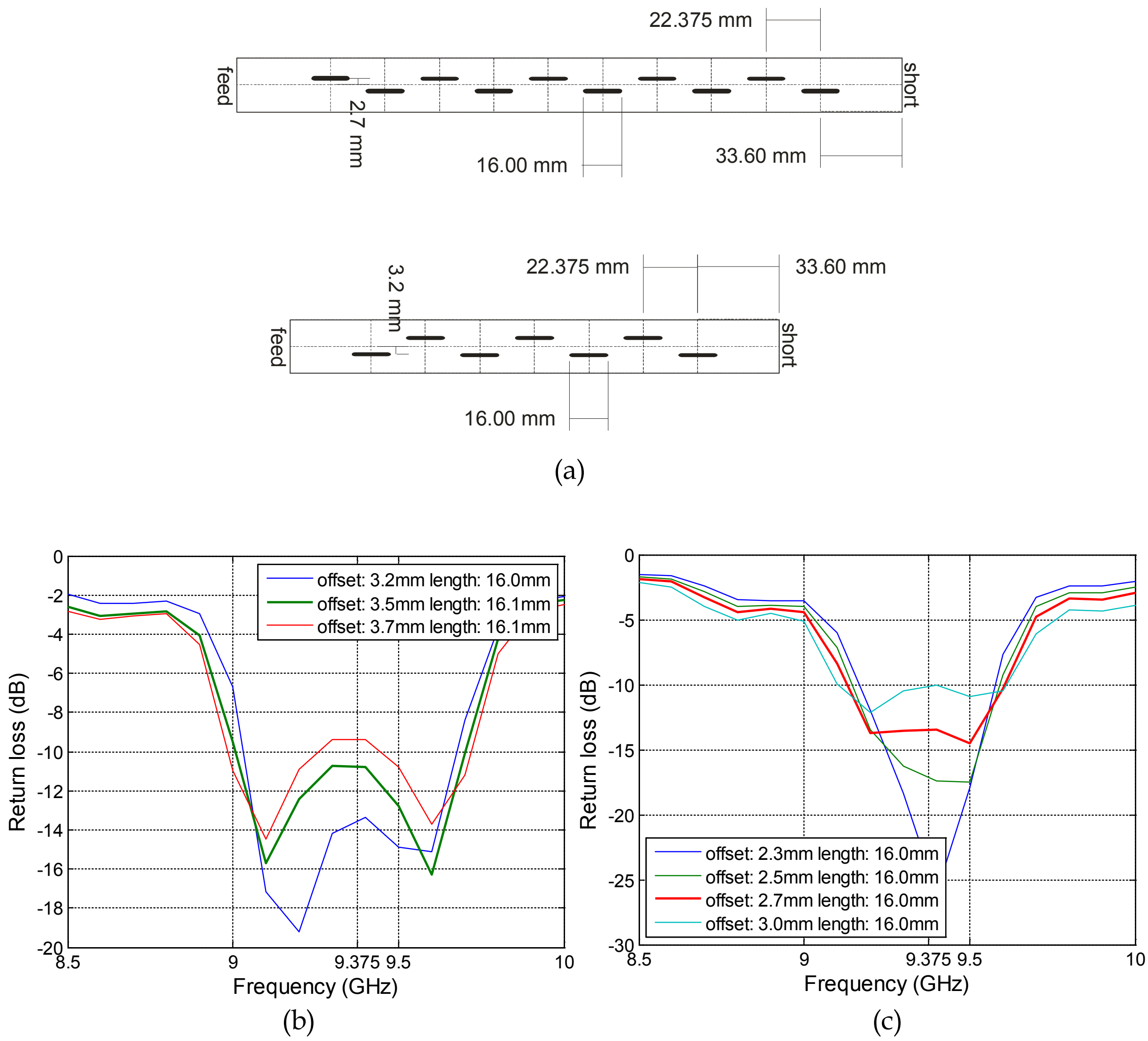

Figure 2-11 (a) Dimensions and return loss as simulated in the single slot design cell FEM model for (b) 7-slot and (c) 10-slot arrays with 3.00 mm wall thickness (typical CFRP aircraft skin)

FEKO™ models of the 10-slot SWA arrays with 0.50 mm and 1.27 mm wall thickness were simulated. These models used the slot length/offset for the 0.50 mm CFRP and 1.27 mm aluminium alloy designs. However in all MoM models the waveguide walls were simulated as a perfect electrical conductor (PEC). It is known that the electrical properties of CFRP are complex and not well understood so not incorporating them into the CFRP simulations was a substantial simplification. In Section 2.9 it is discussed that this simplification was most likely the cause of differences between the measured and MoM simulated return loss.

The simulated three dimensional far-field radiation pattern for a 10-slot array with 1.27 mm thick PEC walls is shown in Figure 2-12. This is typical of the radiation pattern for all multi-slot SWA arrays in the far field at resonance (9.375 GHz). The E-plane (transverse to waveguide axis in Figure 2-12) radiation pattern was broad while the H-plane (parallel to waveguide axis in Figure 2-12) radiation pattern was a highly directive with a well-defined main lobe and side lobes. The antenna was linearly polarised transverse to the waveguide axis of Figure 2-12.

The MoM simulated antenna patterns for the two 10-slot arrays across a 10% bandwidth are shown for the E-plane in Figure 2-13 and H-plane in Figure 2-14. All of these plots were normalised to 0 dB in the 0° (broad-side) direction. The E-plane radiation pattern was the characteristically broad lobe in the plane transverse to the waveguide axis. The simulated H-plane radiation patterns showed the same shape progression as in the published radiation patterns of [28] and the characteristic significant change for a high-Q resonating cavity across a 10% bandwidth. Specifically, at the design frequency of 9.375 GHz, the simulation showed a well-defined main lobe and symmetrical side lobes. Below and above the design frequency, it showed a null in the bore-sight direction (split beam).

Frequency scanning, where beam direction changes with frequency, is a characteristic feature of resonant SWA arrays. In some situations it may be exploited to provide a beam steering functionality while in other situations it introduces errors in the antenna direction. The MoM simulations for the 10-slot SWA arrays were analysed to determine the beam direction, expressed as the angle of peak gain from bore-sight (angle = 0°) in the E- and H-planes. The simulation results are shown in Figure 2-15.

The E-plane beam direction was within 1° of bore-sight from 9.2 to 9.7 GHz (5.3% bandwidth). At frequencies outside this range, the beam direction was very sensitive to frequency as demonstrated by the peaks at 8.8, 9.0, 9.8, 10.3, 10.4 and 10.5 GHz. This variable effect means that beam steering by frequency scanning in the E-plane would not be practicable.

In contrast, the angle of peak gain in the H-plane rose almost linearly from -9° at 8.5 GHz, through 0° at 9.375 GHz to +8° at 10.3 GHz. Beam steering in this plane using frequency scanning should be straightforward.

The angle of peak gain for both the 0.50 and 1.27 mm wall thickness designs in both principal planes were in reasonable agreement across the entire 8.5 to 10.5 GHz frequency band. This provides further confidence that the two designs were equivalent, despite the difference in slot dimensions.

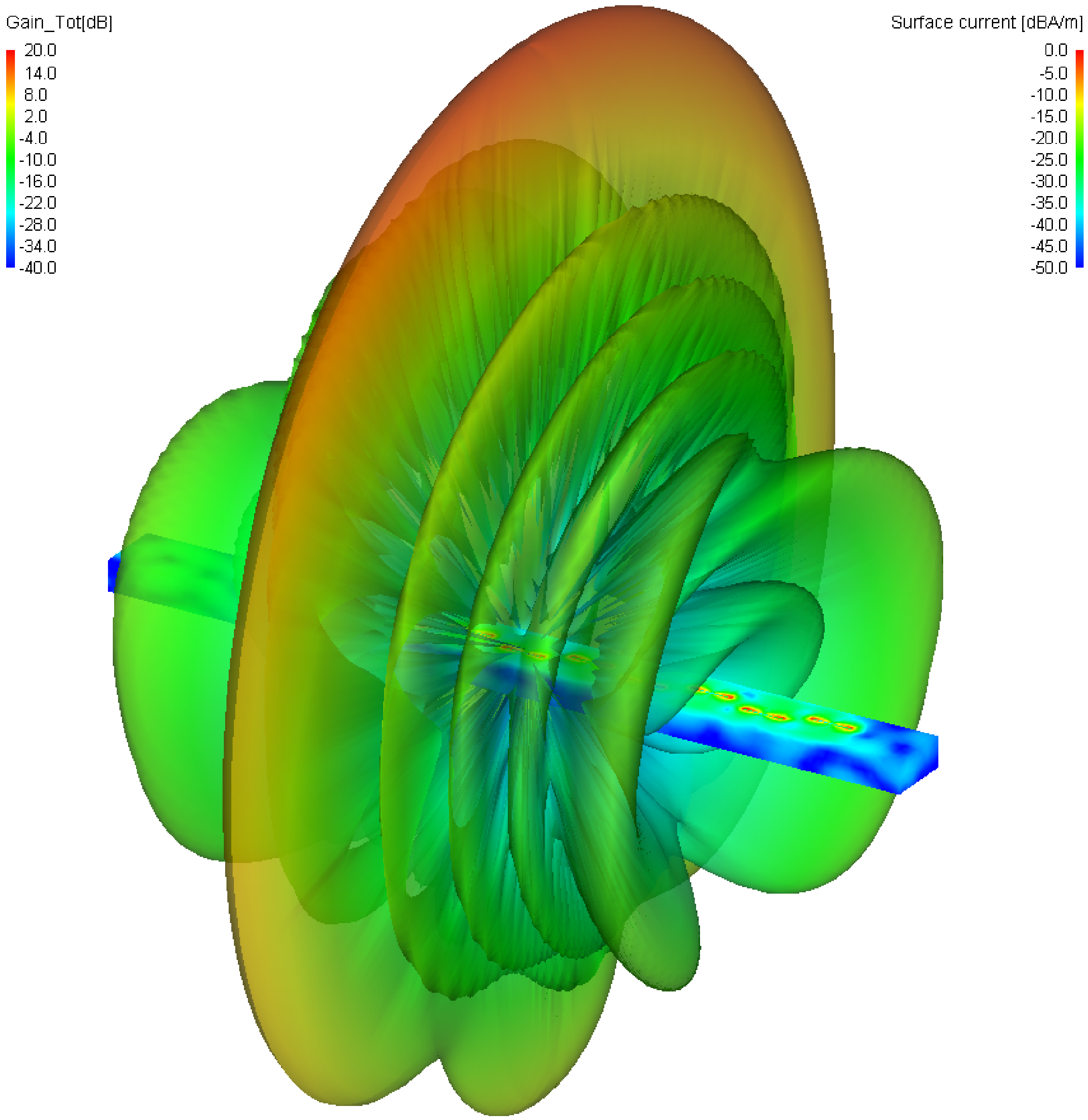

Figure 2-12 MoM simulated current distribution on the exterior of the waveguide and three dimensional radiation pattern from the 10-slot SWA array with 1.27 mm thick PEC walls at 9.375 GHz

2.8. Manufacture and test of selected arrays

CFRP waveguides were manufactured from IM7/977-3 unidirectional prepreg tape (Hexcel Corporation) wrapped over aluminium alloy mandrels. The effective dimensions of the mandrels when covered with release agent were approximately 330 mm x 22.8 mm x 10.1 mm. The inner cross-section of the cured CFRP waveguides was typically within 0.1 mm of the 22.86 mm x 10.16 mm inner dimensions specified for rigid rectangular WR-90 waveguide. The manufacture process is summarised in the following six bullet points:

- The roll of uncured prepreg tape was removed from the freezer, allowed to thaw then the plies cut. The size of each ply was set to be as close as practicable to perfectly circumferential with a perfect butt-joint between the ply ends. The aim was to have each ply as close to parallel to the applicable waveguide wall with a minimum of disruption at the seams. The seam was located on the broad wall centre line, alternating sides for each ply.

- Prepreg plies with the fibres oriented longitudinally along the waveguide axis were defined as 0° plies and those with fibres oriented circumferentially around the waveguide were defined as 90° plies. The ply stacking sequence was $[0\ 90]_S$ where the waveguide inner wall was at 0°.

- Each prepreg ply was wrapped over the mandrel, or previous ply, covered with a hard outer tool and vacuum bag debulked for at least five minutes before applying the next ply. The inner 90° plies tended to pull-away from the mandrel so care was required when wrapping to ensure that all fibres maintained the correct orientation when setting up for debulking.

- The wrapped mandrel was vacuum bagged and autoclave cured using the manufacturer recommended cure cycle of 177 °C/586 kPa for 6 hours with heating and cooling rates of 3 °C/min. A -100 kPa vacuum was applied at the start of the cycle until the autoclave achieved a positive pressure of +100 kPa.

- After curing, the waveguides were slid out of the mandrels. Sharp edges were removed using wet/dry abrasive paper and waveguides were cut to length with a water lubricated diamond saw. The final waveguide wall thickness was approximately 0.5 mm.

- The slots were cut in the CFRP waveguide using a MultiCAM M-I Computer Numerically Controlled (CNC) Router and a 1.0mm diameter diamond coated end mill. The CNC spindle speed was set to 15,000 revolutions / minute with a feed rate of 10 mm / minute, plunge speed of 1 mm / minute and pass depth of 0.1 mm.

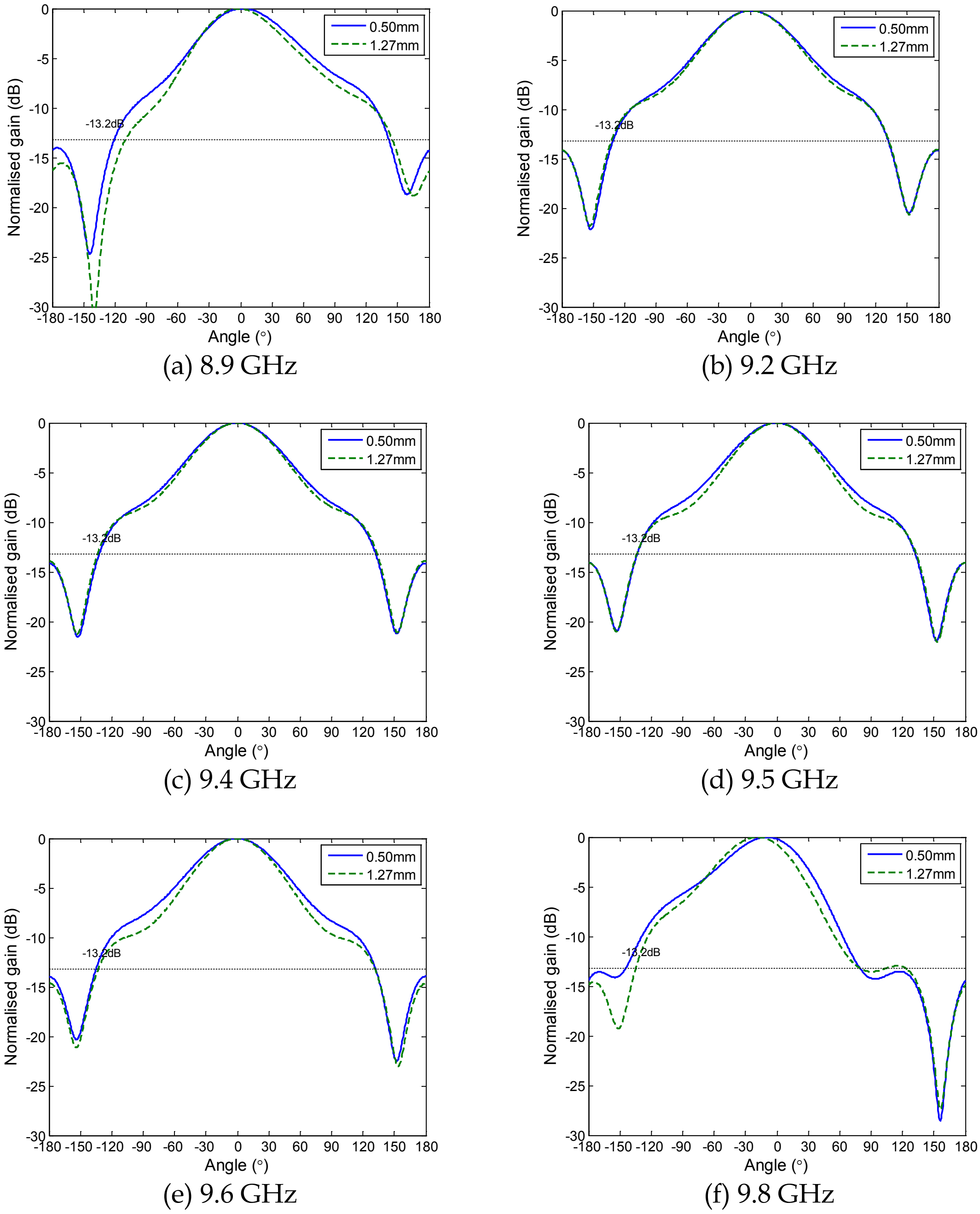

*Figure 2-13 MoM simulated **E**-plane antenna patterns of 10-slot SWA with 0.5 mm and 1.27 mm thick PEC walls across 10% bandwidth*

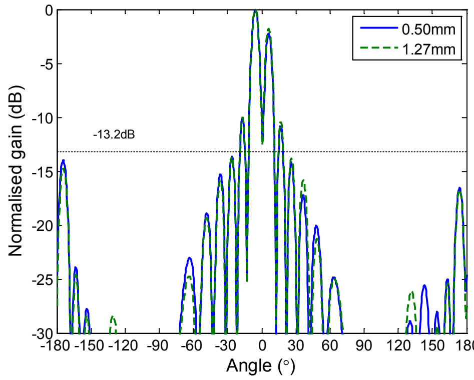

(a) 8.9 GHz

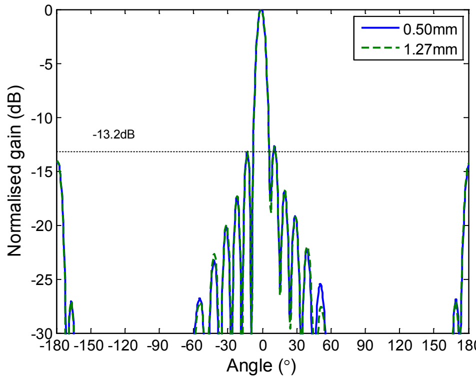

(b) 9.2 GHz

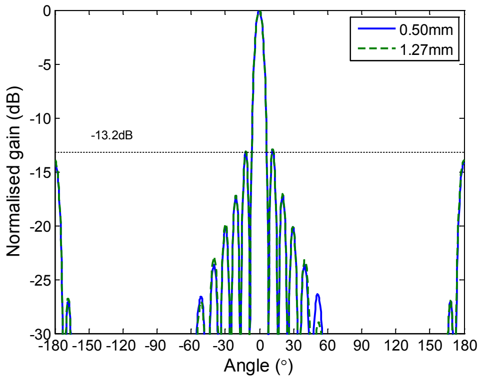

(c) 9.4 GHz

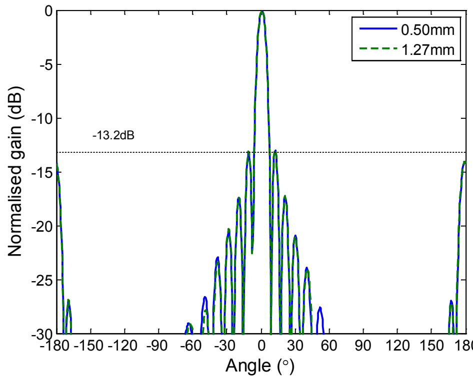

(d) 9.5 GHz

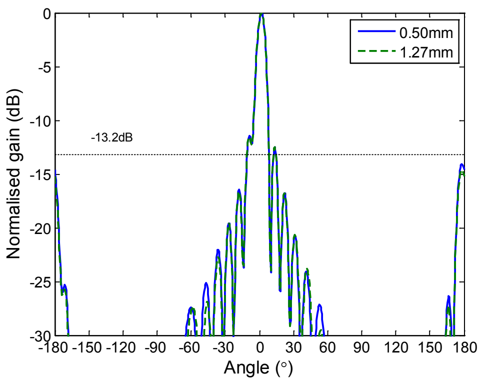

(e) 9.6 GHz

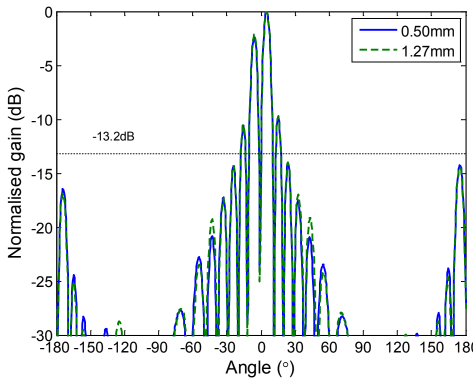

(f) 9.8 GHz

Figure 2-14 MoM simulated ***H****-plane antenna patterns of a 10-slot SWA array with 0.5 mm and 1.27 mm thick PEC walls across 10% bandwidth*

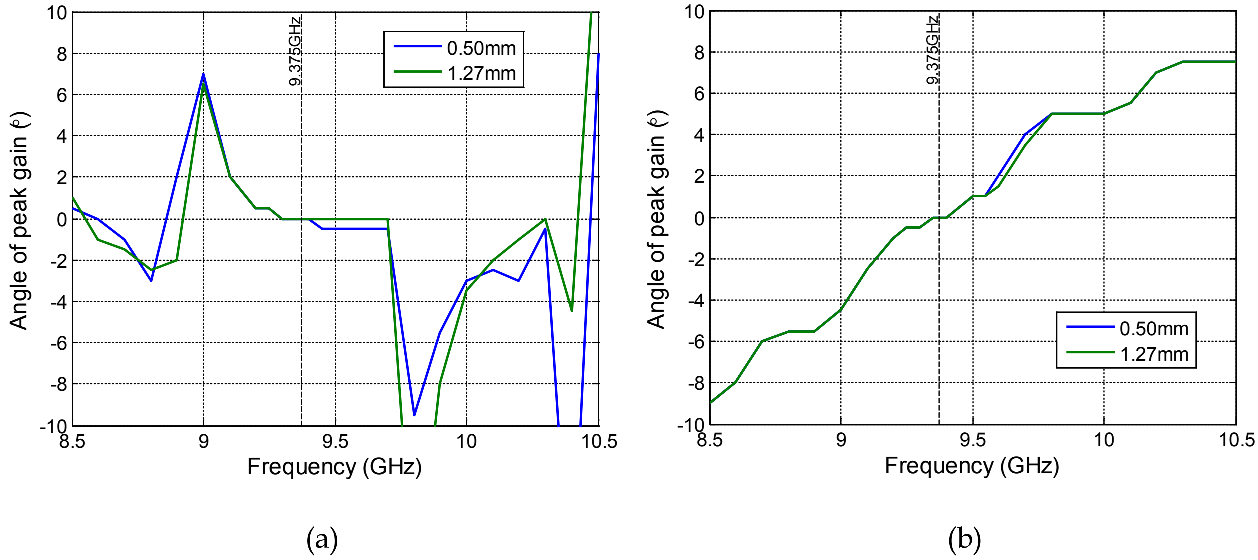

Figure 2-15 MoM simulated effect of frequency and PEC wall thickness on beam direction (angle of peak gain from bore-sight) in the (a) E- and (b) H-plane for the 10-slot SWA arrays

Aluminium alloy arrays were manufactured from standard rigid rectangular aluminium alloy WR-90 waveguide with a wall thickness of 1.27 mm supplied by Penn Engineering. The waveguide was cut to length on a conventional mill and the slots machined using the CNC router. To achieve a good edge finish, it was necessary to centre drill the slot ends prior to machining the slot length.

Waveguide flanges were bonded to the feed end and metal shorting blocks to the termination end. Aremenco Bond 525 conductive epoxy was used to ensure good electrical connection between the flange, SWA and shorting block. Photographs of the completed 10-slot aluminium alloy and CFRP arrays are shown in Figure 2-16.

The performance of each manufactured SWA was measured using a Wiltron 360 Vector Network Analyser. A short-open-load coaxial calibration was used to measure the SWA return loss. A simple transmission calibration was used to measure the E- and H- plane antenna gain patterns relative to a Sunol Sciences broadband horn with known antenna gain. Antenna gain patterns were measured in a microwave anechoic chamber.

2.9. Correlation of experimental results with simulations

2.9.1. Results summary

Table 2-2 summarises the experimental measurements and simulations made in this work and should be referred to when considering the remainder of Section 2.9.

2.9.2. Return loss discussion

The measured and simulated (MoM) return loss for the 7- and 10- slot SWA arrays are shown in Figure 2-17. The aluminium alloy (1.27 mm wall thickness) and CFRP (0.5mm wall thickness) were modelled as PEC. Direct comparison between the MoM simulated return loss for aluminium alloy (1.27 mm wall thickness) and the measured equivalent was possible. The comparison between the measured CFRP (0.5 mm wall thickness) and simulated PEC (0.5 mm wall thickness) will be discussed later in this Section.

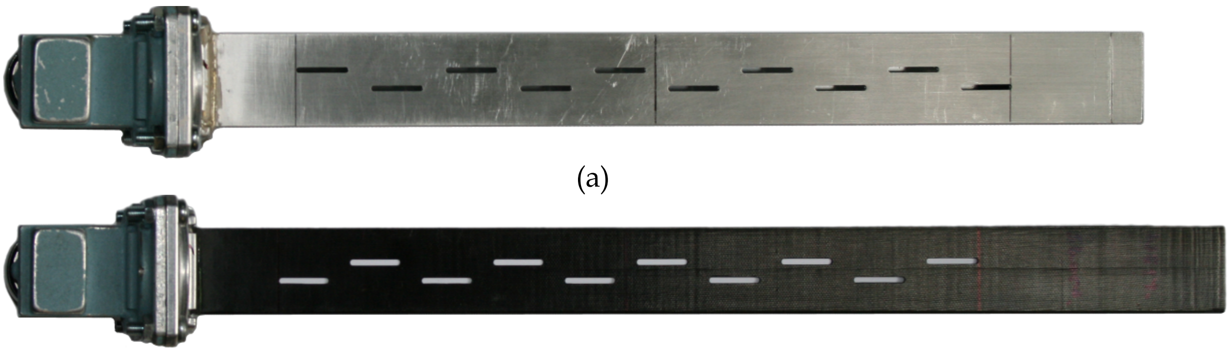

(a)

(b)

Figure 2-16 Photographs of the manufactured 10-slot (a) aluminium alloy and (b) CFRP SWA arrays with Maury Microwave coax-to-waveguide adapters

Table 2-2: Measured (CFRP and aluminium alloy) and simulated (PEC) performance of the SWA arrays considered in this report

	7-Slot				**10-Slot**			
	0.5 mm		*1.27 mm*		*0.5 mm*		*1.27*	
	Measured	*Simulated*	*Measured*	*Simulated*	*Measured*	*Simulated*	*Measured*	*Simulated*
RL[1] (dB)	-25.5	-13.4	-11.2	-10.7	-17.5	-16.8	-17.1	-17.7
BW[2] (%)	5.5	6.3	7.2	7.1	3.5	4.4	5.5	4.1
PG[3] (dB)	Not measured				14.1	16.6	16.5	16.7

Notes:

1 Return loss (RL) as measured at 9.375 GHz.

2 Bandwidth (BW) calculated as $\left(\frac{f_{high}-f_{low}}{f_{centre}}\right)\times 100$ where f_{high} and f_{low} are the -10 dB return loss bounds and $f_{centre} = f_{low} + 0.5\times\left(f_{high} - f_{low}\right)$.

3 Peak gain (PG) measured in the bore-sight direction (0°) in the resonant frequency of 9.375 GHz.

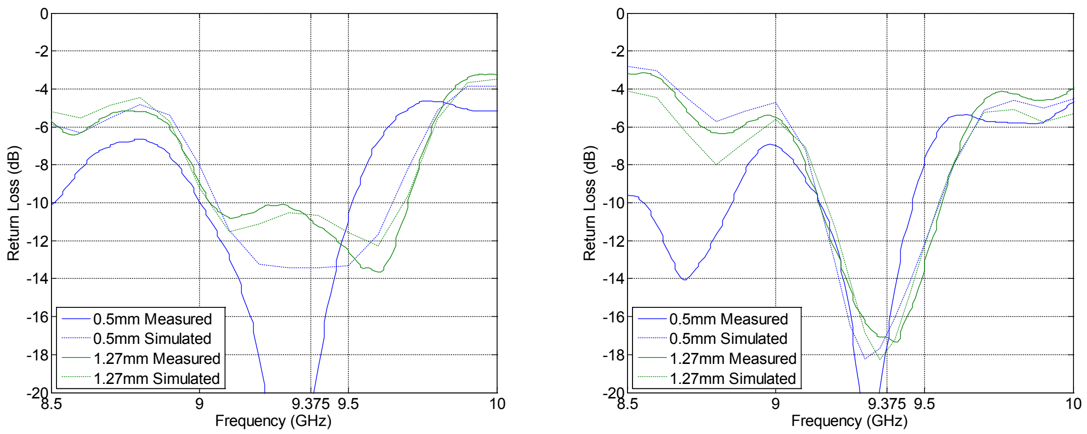

(a) (b)

Figure 2-17 Measured and simulated (MoM) return loss for (a) 7-slot and (b) 10-slot single stick SWA

The shape of these return loss plots are characteristic of resonant slot arrays. RF energy is retained within the waveguide except close to the resonant frequency where there is strong coupling through the slots and out into free space. There was good agreement between the measured and simulated return loss for the 1.27 mm (aluminium alloy) 7- and 10-slot SWA. Thus the MoM simulation accurately modelled the interaction between the standing wave within the short circuit terminated waveguide and the slots in the broad wall.

It was also noted that the MoM simulated return loss for the PEC 0.5 mm and 1.27 mm wall thickness arrays (dotted curves in Figure 2-17) were similar. This similarity, despite the different slot lengths/offsets used in the designs, provided added confidence in the RF design methodology. The simulations indicate that the net power radiated by 0.5 mm and the 1.27 mm PEC SWA with the same number of slots was similar.

The bandwidth (frequency range over which $S_{11} \leq -10$ dB) of the 7-slot arrays was wider compared to the equivalent 10-slot arrays. This is in accordance with the design criteria for each array. The aluminium alloy 10-slot SWA exhibited a measured bandwidth of 5.5% whereas the CFRP resonant SWA exhibited reduced bandwidth of 3.5%. Away from the target frequency of 9.375 GHz and the well matched band of the antenna, the return loss of the CFRP antennas was significantly lower due to the poor conductivity of the CFRP waveguide.

Across the X-band, the effective conductivity of quasi-isotropic CFRP is $\approx 30 \times 10^3$ S m^{-1} and aluminium alloy is $\approx 10 \times 10^6$ S m^{-1}. This leads to a measured insertion loss in WR-90 waveguides of approximately 4.8 dB m^{-1} for CFRP and 0.13 dB m^{-1} for aluminium alloy [2, 3, 4, 30]. A simplistic analysis would suggest that the 30 cm CFRP waveguides tested in this work should be 2.8 dB (= (4.8 - 0.13) x ((30x 2))/100)) more lossy than the aluminium alloy waveguide. The factor of 2 arises because the wave must travel down the waveguide, reflect off the short, then return to the feed. However Figure 2-17 shows that this difference varied between -8 and +10dB.

A finite isotropic wall impedance of 30 x 10^3 S m^{-1} was assigned to the MoM waveguide model as a first approximation to the poor conductivity of CFRP (0.5 mm wall thickness) waveguides. The simulated return is compared with the measured return loss in Figure 2-18.

For the 7-slot SWA array, the finite impedance provided a good approximation to the measured return loss for frequencies below resonance. At resonance, the finite impedance failed to capture the complex Ohmic and dielectric losses present in the CFRP. At frequencies above resonance, there is qualitative agreement between the measured and finite impedance simulation. For the 10-slot array, the finite impedance simulation better approximated the measured return loss compared to the PEC simulation in Figure 2-17. However, it is clear that a simple isotropic finite impedance is insufficient to accurately capture the loss within a CFRP waveguide. This behaviour was not investigated further.

2.9.3. Peak gain discussion

The measured and predicted peak gain for the 10-slot arrays are shown in Figure 2-19. The prediction for the 10-slot aluminium alloy array was excellent. At resonance the peak gain was predicted to be 16.7 dB and measured as 16.5 dB.

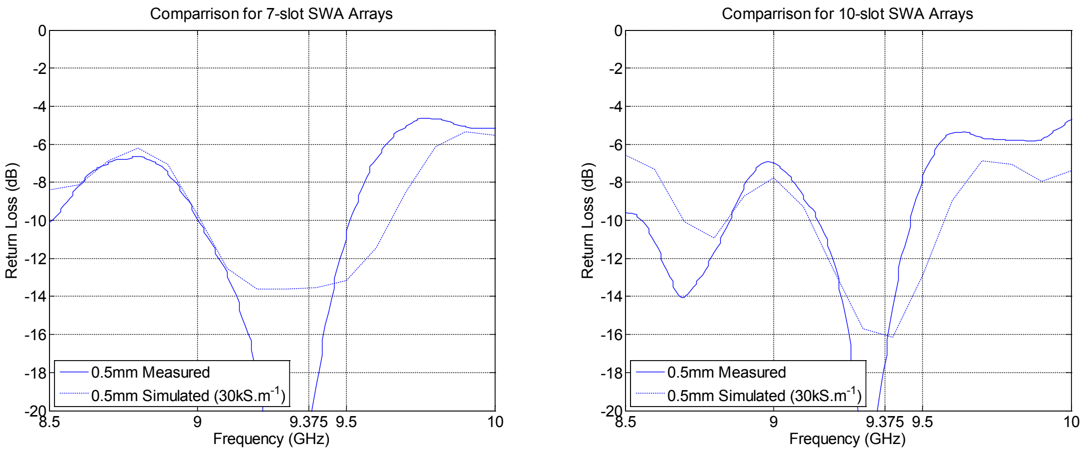

(a) (b)

Figure 2-18 Measured and simulated (MoM) return loss for the (a) 7- and (b) 10-slot SWA with a finite wall impedance of 30 x 10^3 S m^{-1}

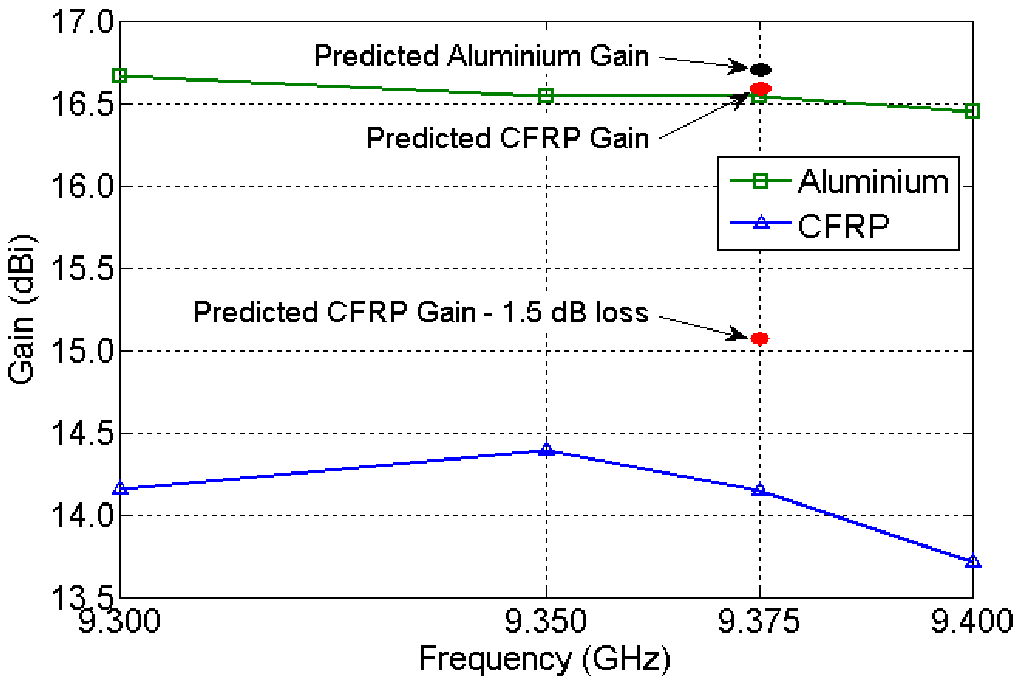

Figure 2-19 Effect of frequency on the measured peak gain for 10-slot SWA in aluminium alloy and CFRP

The predicted peak gain of the 10-slot CFRP array did not match the measured peak gain. At resonance the peak gain was originally predicted to be 16.6 dB and measured as 14.1 dB. The prediction assumed a PEC wall and it was hypothesised that the difference may be caused by Ohmic and dielectric losses because of the poor conductivity of the CFRP waveguide. In the previous section it was calculated that the difference in attenuation loss between the 30 cm long CFRP and aluminium alloy arrays could be up to 1.5 dB. Even when the predicted gain was reduced by this margin (16.6 dB – 1.5 dB = 15.1 dB) there was still an approximately 1 dB difference.

This additional loss may be due to the combination of (i) non-uniform impedance within the CFRP and (ii) currents flowing in the through-thickness direction at the ends of the slots. With regard to (i), the complex conductivity of unidirectional CFRP is strongly dependant on fibre orientation. When CFRP plies are stacked in a laminate, the through-thickness impedance becomes very difficult to model. With regard to (ii), the currents in resonant slot antennas are highest at the ends of the slots (see Figure 2-12) and there are significant components of this current in the through-thickness direction. This hypothesis will be tested in the future.

The MoM simulated effect of frequency on peak gain was similar for the 7- and 10-slot SWA for both wall thicknesses. This was expected because both arrays were resonant and designed to be equivalent (i.e. equivalent slot conductance).

2.9.4. Antenna pattern discussion

The radiation patterns of the 0.5 mm thick CFRP and 1.27 mm thick aluminium alloy 10-slot arrays were measured in an anechoic chamber from 9.3 to 9.4 GHz. The measured and MoM simulated H-plane patterns are shown in Figure 2-20 and Figure 2-21. Note the MoM result assumed PEC for both 0.5 mm and 1.27 mm wall thickness. No attempt was made to capture the 30×10^3 S m^{-1} in the simulation of the CFRP (0.5 mm wall thickness) SWA.

Figure 2-20 and Figure 2-21 are classical antenna patterns for resonant arrays - a clear central beam with diminishing side-lobes. For the 0.5 mm and 1.27 mm wall thickness results, the first side lobes were symmetrical and their amplitudes were close to -13.2 dB below the central peak, consistent with the uniform amplitude distribution. Furthermore, the measured back lobes were about -12dB below peak gain in agreement with the MoM simulations.

The measured H-plane radiation pattern for the CFRP (0.5 mm wall thickness) SWA was lower than the MoM prediction. This is consistent with the lower measured return loss (Figure 2-17) and peak gain (Figure 2-19). The MoM simulation did not take into account the complex impedance of the CFRP.

2.10. Preliminary amplitude tapering investigation

It is common to have antenna patterns that are different to that created by arrays of uniform amplitude radiators. For example in some applications it is necessary that the amplitude of the first side lobe be below the 13.2 dB characteristic of uniform amplitude arrays. The usual method of achieving this pattern control is through amplitude tapering. The relative power emitted by each of the radiating elements (amplitude) is controlled so that the phasor sum of these elements yields the desired radiation pattern.

It is expected that the SWA arrays in operational SWASS will be amplitude tapered. It was therefore decided to validate the simulation capability against results presented in the literature. Developing a design capability for non-uniform amplitude distribution will be the subject of future work.

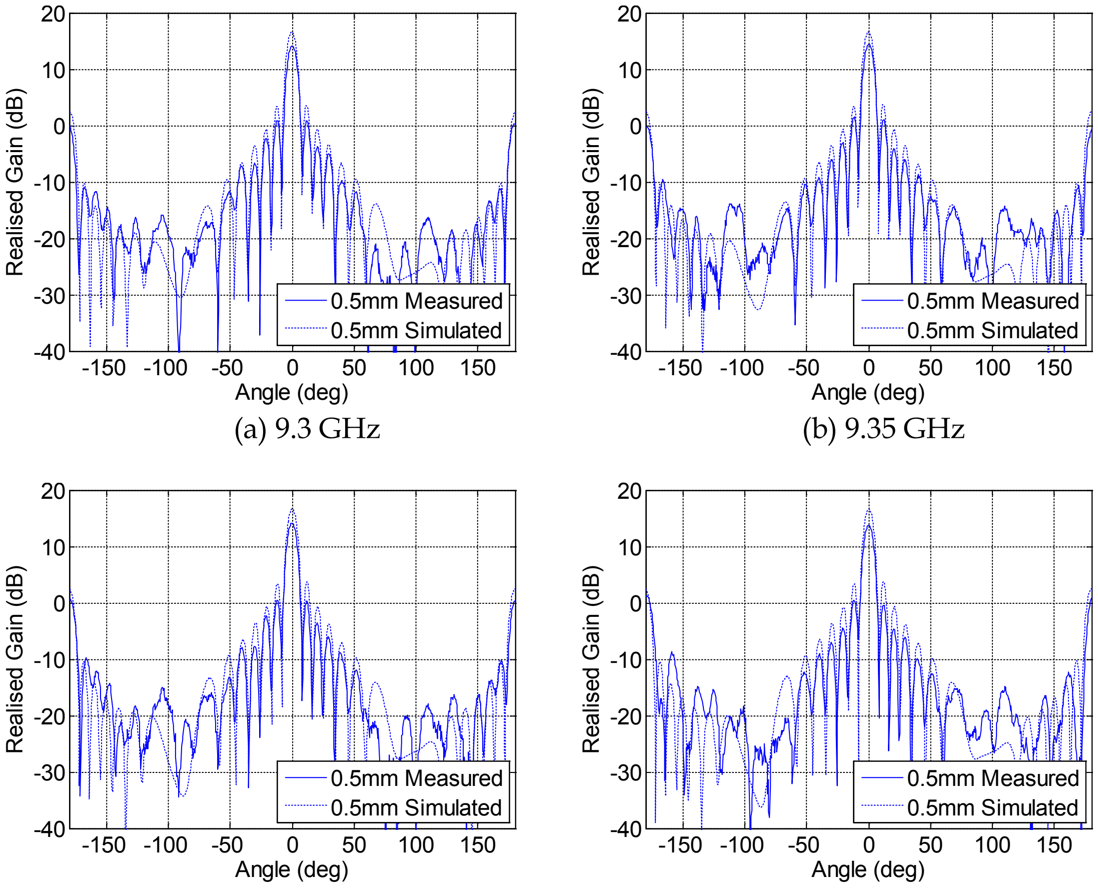

(a) 9.3 GHz (b) 9.35 GHz

(c) 9.375 GHz (d) 9.4 GHz

Figure 2-20 Measured H-plane radiation patterns of 10-slot arrays manufactured from 0.5 mm thick CFRP compared to the simulated MoM model based on PEC

A small number of single-stick resonant SWA arrays with amplitude tapering were identified in the literature [23, 34, 35]. In each of these cases, the design process was detailed.

The array detailed in reference [23] was selected for validation. This was a 10-slot SWA array with 1.27 mm wall thickness and resonance at 9.375 GHz. Amplitude tapering was through a Dolph-Tschebyscheff distribution with a first side lobe level of -26dB. This array was selected in-part because both the design frequency and waveguide wall thickness were identical to that simulated and measured previously (Sections 2.1 to 2.9). The slot lengths/offsets are detailed in Table 2-3 and these may be compared to the 15.7 mm long x 2.5 mm offset used for the 10-slot uniform amplitude array (Table 2-1).

The design from [23] was simulated in FEKO with slot dimensions and offsets specified to four decimal places. However, manufacture of this SWA with four decimal place accuracy is expected to be impractical. Therefore evaluating the effect of manufacture tolerances on the performance of SWASS will be the subject of future work.

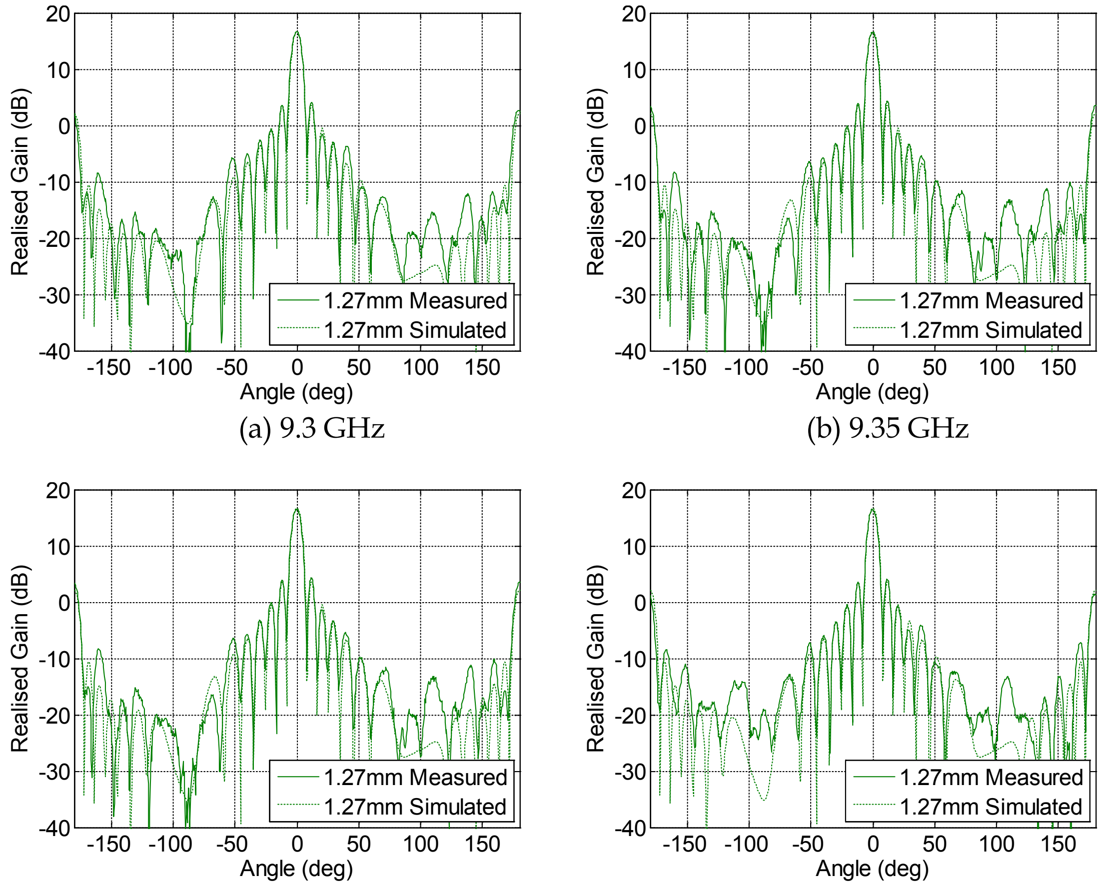

(a) 9.3 GHz (b) 9.35 GHz (c) 9.375 GHz (d) 9.4 GHz

Figure 2-20 Measured H-plane radiation patterns of 10-slot arrays manufactured from 1.27 mm thick aluminium alloy compared to the simulated MoM model based on PEC

Table 2-3 Slot lengths and offsets from Table 1-1 of [23]

Slot number	**Slot length (mm)**	**Slot offset from centreline (mm)**
1 and 10	15.5720	1.0684
2 and 9	15.7077	1.5597
3 and 8	15.7429	2.0913
4 and 7	15.8393	2.7348
5 and 6	15.8993	3.0440

Regardless, the simulated return loss bandwidth ($S_{11} \leq -10$ dB) for both the tapered and uniform aperture distribution designs, shown in Figure 2-21, was identical. Although the amplitude tapering had reduced the side lobe level from -13.2 dB to -26 dB it was predicted to have no adverse effect upon the return loss performance.

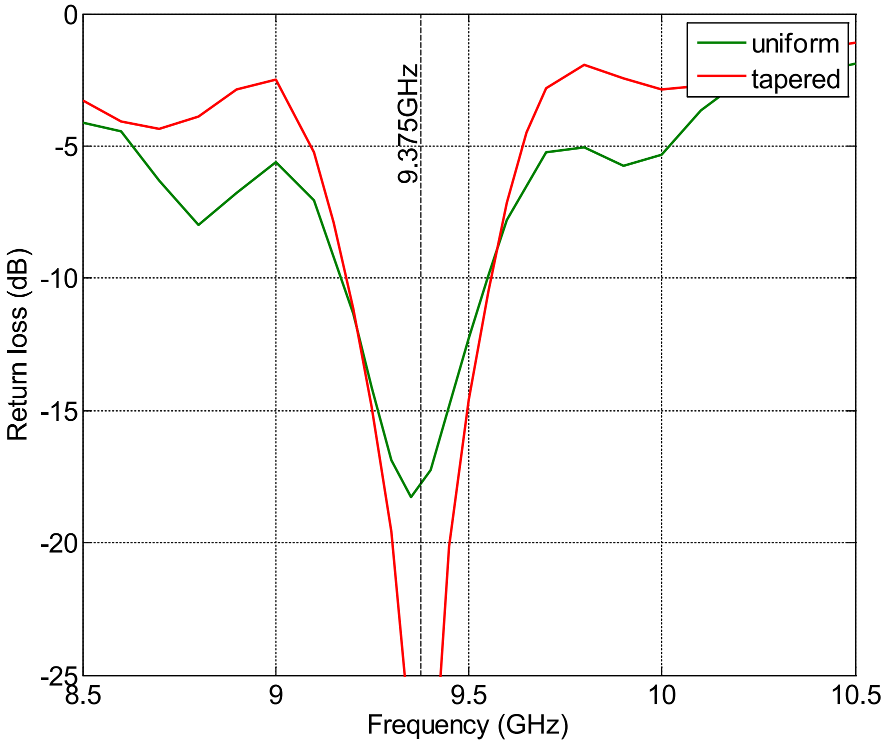

Figure 2-21 MoM simulated return loss for 10-slot SWA arrays with 1.27 mm wall thickness and uniform and -26 dB Dolph-Tschebyscheff distribution

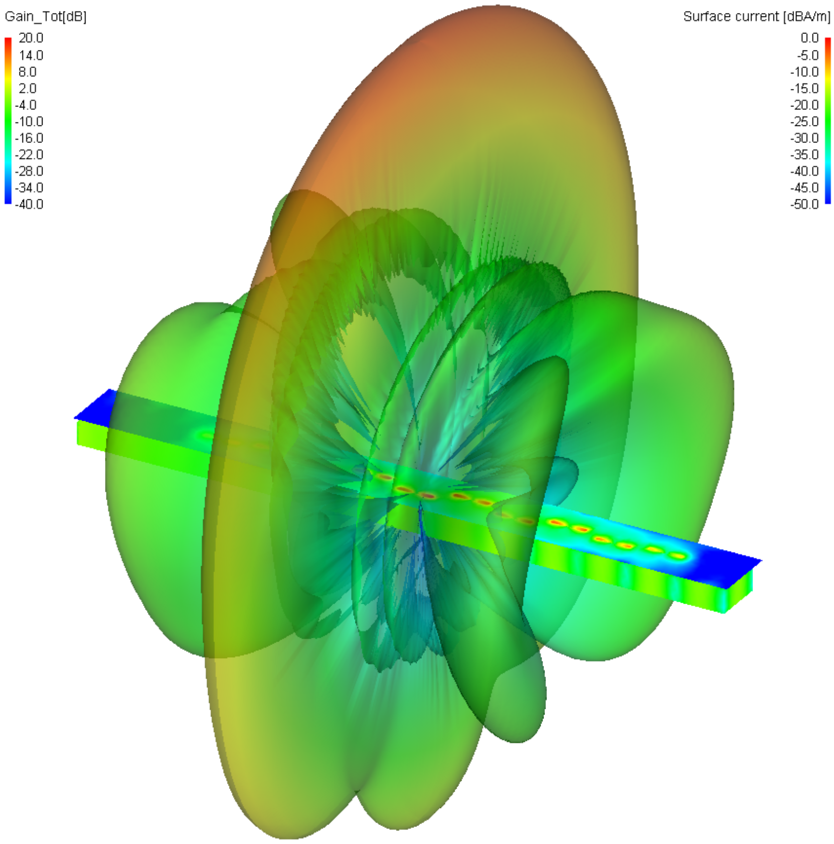

Figure 2-22 MoM simulation of current distribution on inside waveguide wall and top face with radiation pattern for 10-slot SWA arrays with 1.27 mm wall thickness and -26 dB Dolph-Tschebyscheff distribution at 9.375 GHz

The effects of tapering was most apparent in both the current distribution (where the current strength was greatest at the centre of the antenna and minimal at either end) shown on the waveguide in Figure 2-22 and the H-plane antenna patterns shown in Figure 2-23. Clearly the side lobe levels in the amplitude tapered array are much lower compared to those of the uniform aperture distribution (Figure 2-21). The simulated side lobe levels were below -25 dB relative to peak gain, in agreement with the design from [23].

Experimental measurement of the antenna pattern will be conducted will be conducted in the future in order to validate the simulation. In [23] the measured side lobe level at 9.375 GHz was only -16 dB rather than the designed -26 dB. It is suspected that this difference was a result of manufacturing tolerances.

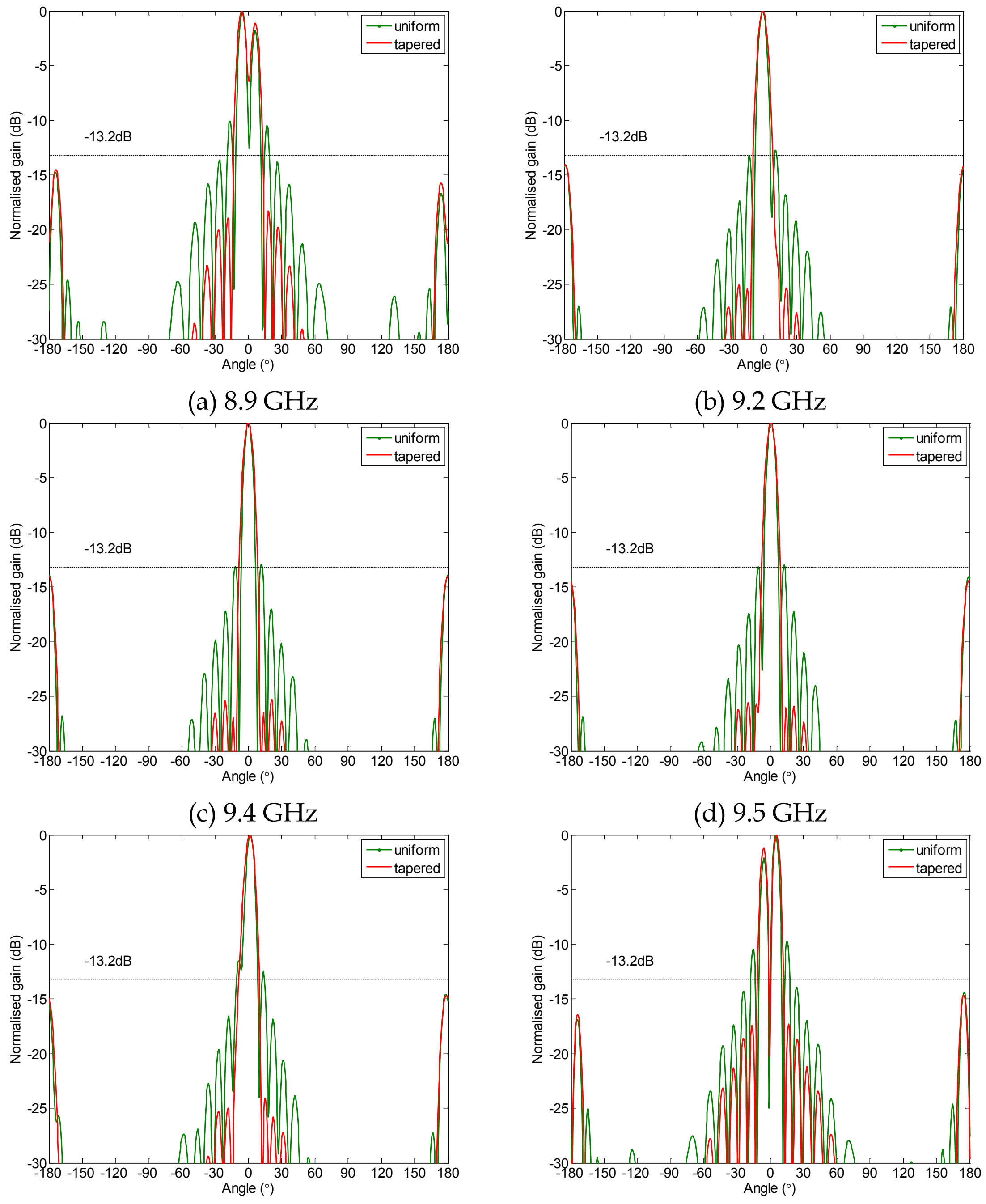

(a) 8.9 GHz (b) 9.2 GHz

(c) 9.4 GHz (d) 9.5 GHz

(e) 9.6 GHz (f) 9.8 GHz

Figure 2-23 MoM simulated H-plane radiation patterns of 10-slot SWA arrays with 1.27 mm wall thickness and uniform and Dolph-Tschebyscheff distributions across a 10% bandwidth

3. Plug-and-loop RF feed

3.1. Aim

It is necessary to feed RF energy into the SWASS waveguides. The feeding device must:

- allow adjacent waveguides to be fed,
- be acceptably simple and robust to manufacture and install, and
- not require intimate physical or electrical contact with the waveguide walls.

The plug-and-loop design shown in Figure 1-8 was devised to satisfy these constraints. The plug supports the loop and may be slid into the end of CFRP waveguides. It contained an integral low-high impedance choke to minimise losses through the gap between the waveguide wall and plug. An SMA connector was fastened to the plug and soldered to the loops. The loop was manufactured from brass shim and its dimensions adjusted to give the widest possible bandwidth with minimal return loss at the design frequency.

The first generation of plug-and-loop feeds were manufactured from aluminium alloy and brass. This was satisfactory to demonstrate the concept. However the configuration and materials (a solid block of aluminium alloy or a sheet of brass shim) would not be suitable for SWASS aircraft components. Aluminium alloy is vulnerable to galvanic corrosion in the presence of CFRP and aircraft manufacturers expend considerable effort to develop procedures that will ensure these materials are electrically isolated. In addition the plug would support very little structural loads so manufacturing it from a solid block of material would add redundant weight. It is possible that the brass shim loop may not be sufficiently stiff to retain its shape. Future work in the SWASS program will be directed at designing a plug from the same thin CFRP laminate as used in the waveguide walls and a robust loop.

The plug-and-loop concept was validated by measuring the effect of brass shim width and loop length on RF loss and bandwidth in a CFRP waveguide as detailed in the remainder of Section 3.

3.2. Loop feeds in the back-to-back configuration

The L-probe feed described in [21] is in intimate electrical contact with the waveguide walls. Hence the instantaneous electrical potential of all parts of this feed are well defined. In contrast the plug-and-loop feed pictured in Figure 1-8 is in imperfect electrical contact with the conducting carbon fibres in the CFRP waveguide because each fibre is encapsulated with an approximately 1 μm thick layer of non-conducting epoxy resin. It was anticipated that this would increase RF losses within the plug-and-loop feed.

The most convenient way of measuring the losses in the plug-and-loop feed was with a back-to-back test piece that could slide into a CFRP waveguide. The back-to-back configuration eased calibration and its geometry, shown in Figure 3-1, consisted of a quarter-wave choke between two blocks. An axial hole contained a short length of RG-402 semi-rigid coaxial cable that was soldered to two identical brass loops located at each end of the plug.

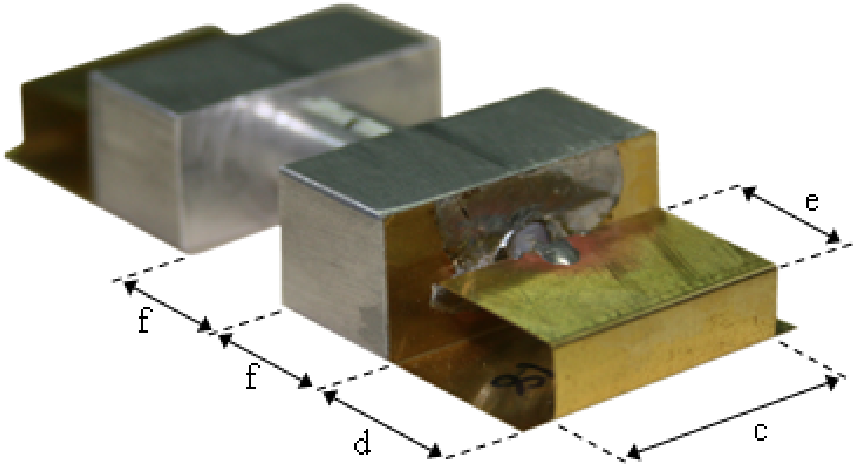

Figure 3-1 Back-to-back test piece geometry

The length of the choke sections were f = $\lambda_g/4$ = 11.2 mm at 9.375 GHz (λ_g = 44.74 mm). The other dimensions (c, d and e from Figure 3-1) were adjusted to optimise RF performance. A c = 1 mm configuration was equivalent to the original wire design of [22] while a c = 18 mm wide loop nearly filled the 22.86 mm width of the WR-90 waveguide and thus was the physical limit for loop width.

All measurements of the back-to-back test pieces were conducted in a 365 mm long length of $[90\ 0]_S$ IM7/977-3 CFRP waveguide (identification code WG18). This waveguide was manufactured using the same technique as described in Section 2.8.

First the S-parameters of the empty CFRP waveguide were measured using a 2-port Thru-Reflect-Line (TRL) calibration with a Wiltron 360 VNA. The S-parameters were then used to calculate the attenuation loss in the empty CFRP waveguide. As shown in Figure 3-2, the attenuation fell from 5.7 dB m^{-1} at 8 GHz to 4.7 dB m^{-1} at 12 GHz. The attenuation as calculated by the Port 1 or Port 2 methods gave near identical loss. These results were in excellent agreement with the attenuation results from prior measurements of shorter CFRP waveguide sections [2, 4, 33].

Seven loop configurations with the dimensions shown in Table 3-1 were then manufactured and tested. Each back-to-back test pieces was slid into the CFRP waveguide and the four S-parameters measured. The loop loss was calculated as the total loss minus the loss for the empty CFRP waveguide at the same frequency (Figure 3-2). Although this approach gave results that were highly dependent upon the return loss (S_{11} or S_{22}), it was judged that this gave a true indication of the loop performance.

The measured S-parameters and return loss are shown in Figure 3-3 to Figure 3-9. Table 3-1 summarises the minimum loss for each loop.

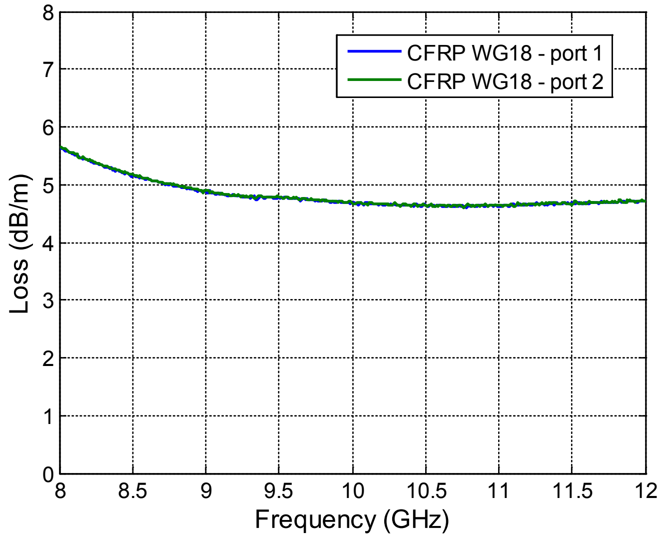

Figure 3-2 Attenuation in a CFRP waveguide with a [90 0]$_s$ ply stacking sequence

Table 3-1 Loop dimensions and RF performance of back-to-back loop configuration in a [90 0]$_s$ IM7/977-3 CFRP waveguide across the X-band

Loop width (c, mm)	**loop length (d, mm)**	**loop top length (e, mm)**	**Minimum back-to-back loop loss (dB)**
1.0	16.5	14.5	0.19
3.0	16.8	14.8	0.20
6.0	16.0	14.0	0.09
9.0	14.8	12.8	0.29
12.0	12.0	14.0	0.24
15.0	11.5	13.5	0.19
18.0	11.25	13.25	0.67

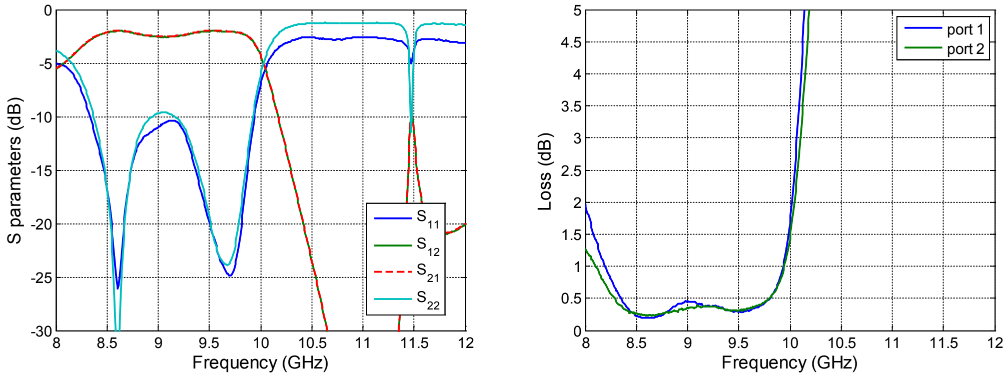

Figure 3-3 Measured S-parameter data and calculated loss of 1 mm wide loops in back-to-back configuration

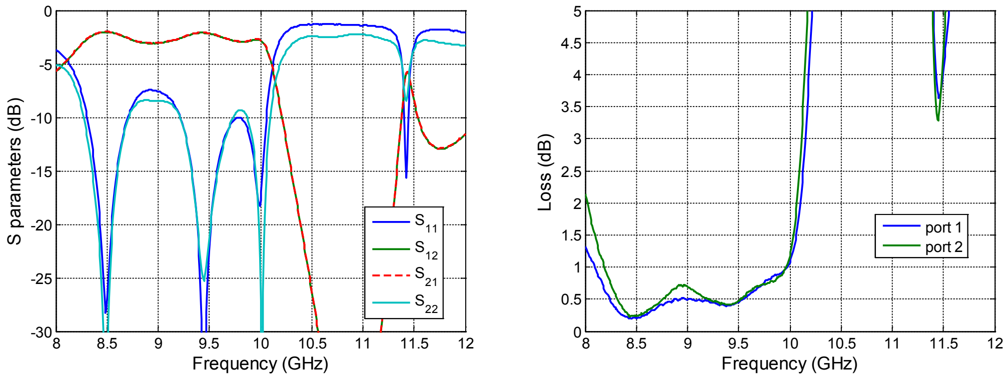

Figure 3-4 Measured S-parameter data and calculated loss of 3 mm wide loops in back-to-back configuration

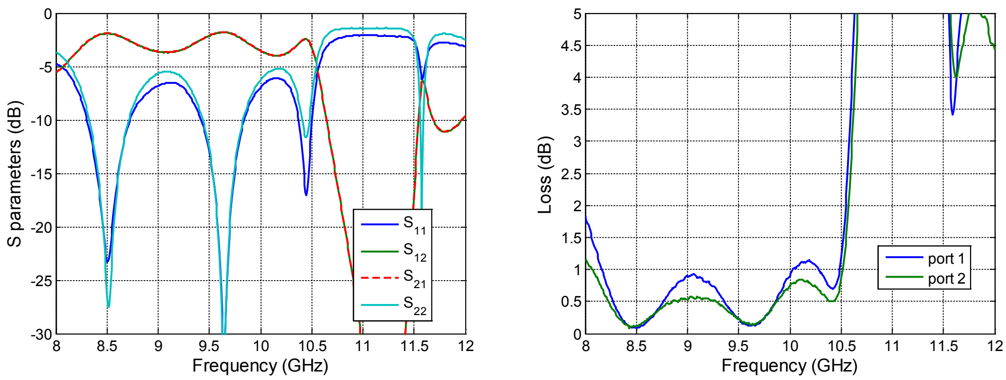

Figure 3-5 Measured S-parameter data and calculated loss of 6 mm wide loops in back-to-back configuration

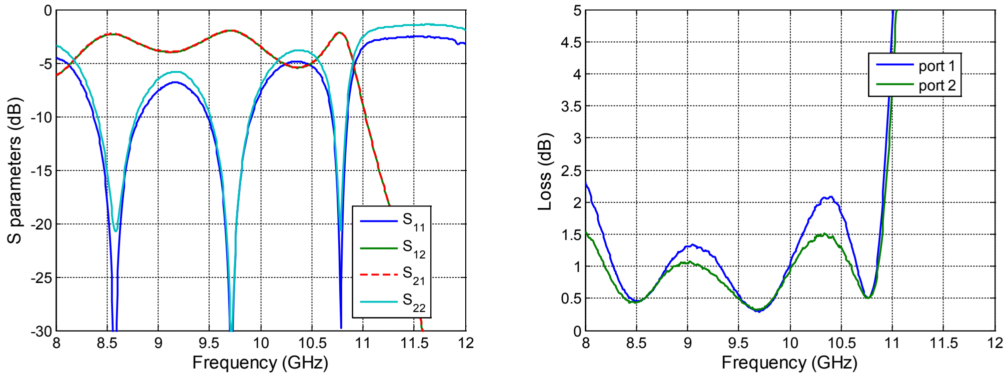

Figure 3-6 Measured S-parameter data and calculated loss of 9 mm wide loops in back-to-back configuration

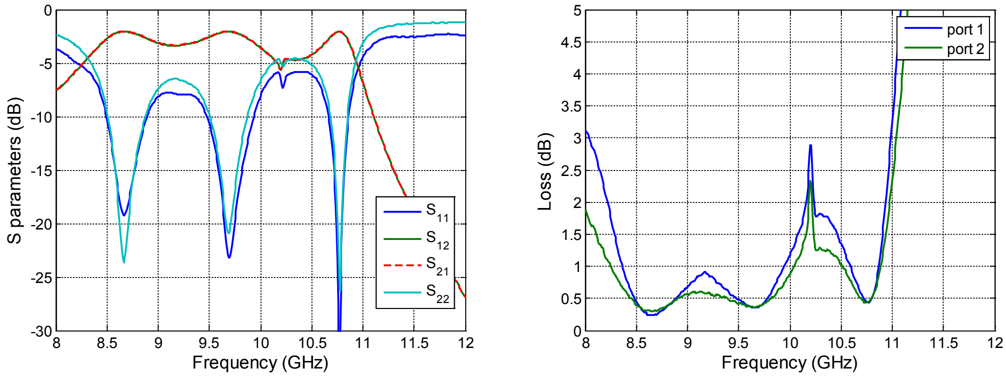

Figure 3-7 Measured S-parameter data and calculated loss of 12 mm wide loops in back-to-back configuration

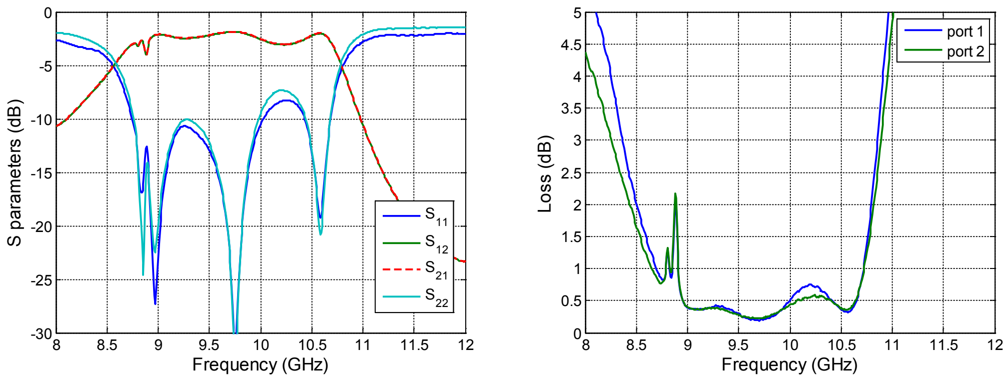

Figure 3-8 Measured S-parameter data and calculated loss of 15 mm wide loops in back-to-back configuration

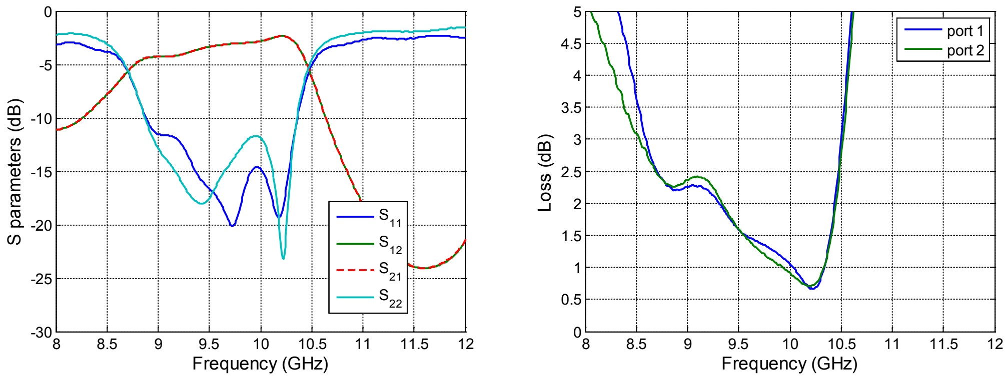

Figure 3-9 Measured S-parameter data and calculated loss of 18 mm wide loops in back-to-back configuration

The minimum and maximum losses for the back-to-back configuration were respectively 0.09 dB for the 6.0 mm wide loop and 0.67 dB for the 18.0 mm wide loop. The loss for all of the remaining specimens ranged from 0.19 to 0.29 dB. If the losses in the short section of RG-402 cable and SMA connector are considered negligible, then the back-to-back specimen loss equated to a single loop loss of 0.10 to 0.15 dB. These losses were considered acceptable for a SWASS feed.

All seven loop designs displayed two or more resonances across the X-band, although only a single resonance was expected. The existence of the multiple resonances indicates that the behaviour of the back-to-back test pieces was more complicated than expected. It is hypothesised that the second resonance was caused by a standing wave within the RG-402 cable. Furthermore, the loss in the back-to-back specimen with the 18 mm wide loop was more than three times greater than in the remainder of the specimens. Simulation of the plug-and-loop feed design would provide insight into the multi-resonant and lossy behaviour and allow for optimisation. However, as stated in Section 3.1, this design was a concept demonstrator only and future work will focus on the development of a CFRP plug. The time and expense of simulation will, if necessary, be directed at the CFRP plugs.

3.3. Plug-and-loop end feeds

In Section 3.2, the loss in the aluminium alloy/brass back-to-back loops were shown to be acceptable for SWASS. To further validate their application to SWASS, seven plug-and-loop end feeds were tested. This is the configuration they would be used in a SWASS panel.

Seven plug-and-loop end feeds were prepared, one for each of the different loop widths evaluated in Section 3.2. These are pictured in Figure 3-10.

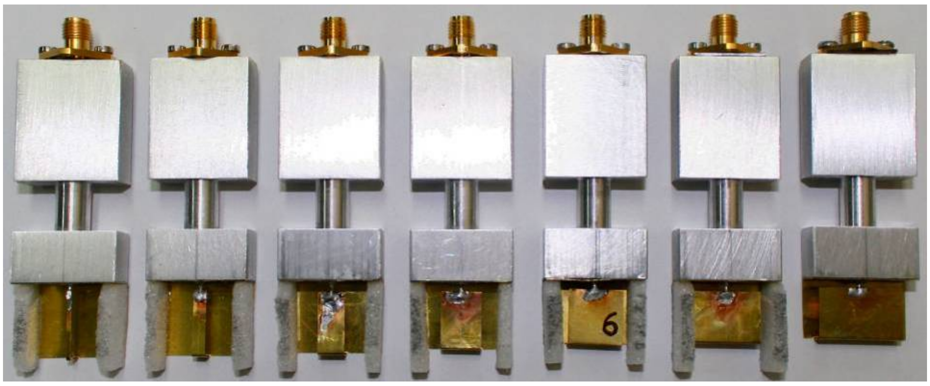

Figure 3-10 Photograph of the plug-and-loop end feed. The 18 mm wide loop is on the right, while the 1 mm wide loop is on the left

Each feed was slid into one end of the IM7/977-3 [90 0]$_S$ CFRP waveguide (WG18) while the other end was terminated with a Maury Microwave Sliding Termination (part no. X314). The return loss was measured with a Wiltron 360 Vector Network Analyser. Theresults are plotted in Figure 3-11 and the bandwidth ($S_{11} \leq -10$ dB) for the plug-and-loop end feed shown in Table 3-2.

All of the loop widths exhibited a single resonance confirming the initial design concept. This is in contrast to the back-to-back configuration where a second resonance was observed.

The resonant frequencies for these loops varied from 9.0 GHz for the 6 mm wide loop to 9.8 GHz for the 15 mm wide loop. If necessary these loops could be tuned to resonate at the target frequency of 9.375 GHz for the 7- and 10-slot SWA arrays. The loop length on the feeds that resonated below the target frequency (1, 6, 12 mm) would need to be shortened while the length of loops on the feeds that resonated at frequencies above the target frequency (3, 9, 15 and 18 mm) would need to be increased.

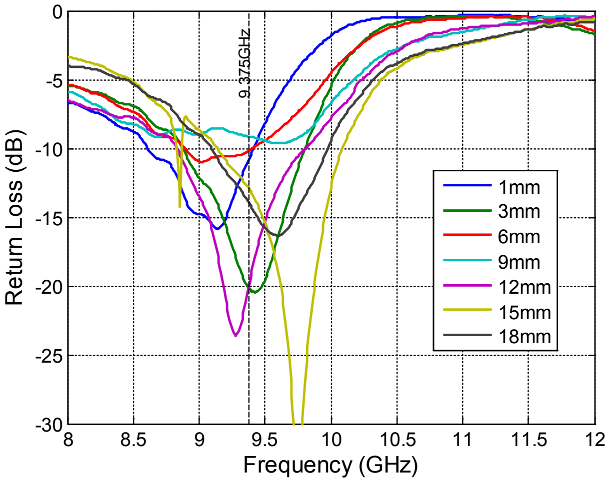

Figure 3-11 Return loss of the plug-and-loop feeds in a CFRP waveguide terminated with a broadband load

Table 3-2 Loop dimensions and RF performance of the feeds in a $[90\ 0]_s$ IM7/977-3 CFRP waveguide across the X-band

Loop width (c, mm)	loop length (d, mm)	loop top length (e, mm)	Loop bandwidth (%)
1.0	16.5	14.5	9.0
3.0	16.8	14.8	10.0
6.0	16.0	14.0	5.7
9.0	14.8	12.8	n/a
12.0	12.0	14.0	10.6
15.0	11.5	13.5	9.9
18.0	11.25	13.25	9.4

All of the loop widths exhibited approximately 10 % bandwidth ($S_{11} \leq -10$ dB). This is substantially wider than the typical bandwidth exhibited by the 7- and 10-slot resonant SWA arrays respectively detailed in Section 2. The exceptions were the 6 mm width loop that possessed only a 6 % bandwidth and the 9 mm wide loop that did not achieve $S_{11} \leq -10$ dB. Thus, any of the loop widths other than 9 mm could be used to feed the resonant SWA arrays from Section 2.

As a final note, it was observed that withdrawing each plug-and-loop feed from the CFRP waveguide made little difference to the return loss even when the high impedance $\lambda_g/4$ section of the choke was fully exposed as shown in Figure 3-12. It was clear that very little RF energy propagated backward out of the gap between the plug and the CFRP waveguide. It is hypothesised that the $\lambda_g/4$ choke section may not be necessary provided that the low impedance $\lambda_g/4$ section fits snugly in the waveguide. This hypothesis will be tested in the future as part of the development of CFRP plugs.

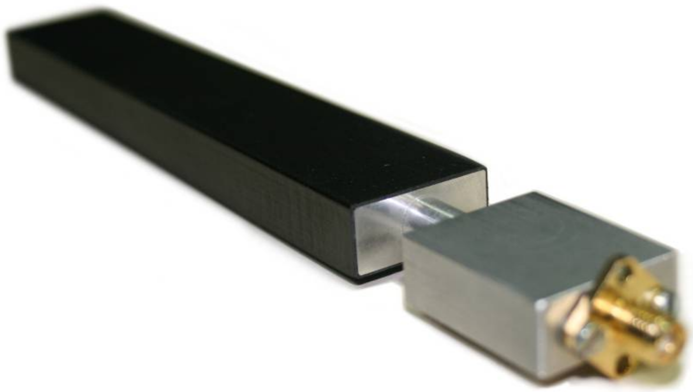

Figure 3-12 Photograph of a plug-and-loop end feed with only the leading edge block inserted in the CFRP waveguide

4. Conclusions

A methodology was developed to design resonant slot waveguide antennas. It used the finite element method and required substantially less computing resources than a Method of Moments simulation. With this model the effect of waveguide wall thickness, slot width, slot length and centreline offset on reflection coefficient were simulated. Multiple iterations were run in order to identify parameter combinations that produced resonant slots. Confidence in the methodology was increased by the very good correlation between its predictions and published data.

This methodology was used to design 7- and 10-slot 9.375 GHz SWA arrays with longitudinal slots in the broad-wall for three wall thicknesses; 1.27 mm standard aluminium alloy waveguide, 0.50 mm aerospace grade CFRP laminates and 3.00 mm thick-skin aircraft panels. Arrays with 0.50 mm thick CFRP and 1.27 mm thick aluminium alloy were subsequently manufactured and tested.

The fabricated SWA arrays exhibited a clear central beam with decreasing side lobes in excellent qualitative agreement with Method of Moments simulations. The correlation between measured and simulated behaviour was considered sufficient to validate the design methodology. The return loss, bandwidth and antenna pattern shape for each array with the same number of slots was equivalent, regardless of the waveguide material. However the gain of the CFRP antenna was much lower compared to the aluminium alloy equivalent because of the significant Ohmic and dielectric losses in the CFRP. Increasing the gain of CFRP SWA would require the conductivity of the inner wall of the waveguide to be improved, which is expected to be straight forward but would increase production and through-life-support costs of SWASS.

A plug-and-loop end feed was developed for use in SWASS waveguides. This device allowed adjacent waveguides to be fed and did not require intimate physical or electrical contact with the waveguide walls. The plug was manufactured from aluminium alloy, supported the brass loop and coaxial connector, and contained an integral low-high impedance choke. It fitted snugly into the end of a waveguide and was bonded in-place with structural adhesive. The effect of loop dimensions on the RF performance was measured. It was found that the feeds had a bandwidth of 10 % and loss of 0.10 to 0.15 dB. This is considered acceptable for a first generation SWASS demonstrator. Future work will focus on developing end feeds that are further integrated into the CFRP structure.

5. Acknowledgement

The authors acknowledge the detailed review of this report by Dr Hedley Hansen (DSTO – Electronic Warfare and Radar Division). His comments and suggestions have assisted with clarity and completeness.

6. References

1. Callus. P. J., "Conformal load-bearing antenna structure for Australian Defence Force aircraft", DSTO-TR-1963, March 2007, 41 pp.
2. Callus. P. J., "Novel concepts for conformal load-bearing antenna structure", DSTO-TR-2096, February 2008, 94 pp.
3. Gray, D., Nicholson, K. J. and Callus, P. J., "CFRP slotted waveguide antenna", *Asia Pacific Microwave Conference 2010*.
4. Nicholson, K. J. and Callus, P. J., "Antenna patterns from single slots in carbon fibre reinforced plastic waveguides", DSTO-TR-2389, August 2009, 34 pp.
5. Silver, S., "Microwave antenna theory and design", P. Peregrinus, London, UK, 1984.
6. Chu, L. J., "Antenna", United States patent 2,479,209, August 16, 1949.
7. Coetzee, J.C., Joubert, J., and Tan, W.L., "Frequency performance enhancement of resonant slotted waveguide arrays through the use of wideband radiators or subarraying", *Microwave and Optical Technology Letters*, Vol. 22, No. 1, July 1999, pp. 35-39.
8. Noble, W.J., and Small, J.W., "Lightweight composite slotted-waveguide antenna and method of manufacture", *United States patent 4,255,752*, March 10, 1981.
9. Wagner, R., and Braun, H.M., "A slotted waveguide array antenna from carbon fibre reinforced plastics for the European space SAR", *Acta Astronautica*, Vol. 8, No. 3, March 1981, pp. 273-282.
10. Miles, P., and Francis, D.R., "Carbon fibre reinforced plastic waveguide elements", *Great Britain patent 2,193,381*, February 3, 1988.
11. Knutsson, L., Brunzell, S., and Magnusson, H., "Mechanical design and evaluation of a slotted CFRP waveguide antenna", *Proceedings of the Fifth International Conference on Composite Materials*, San Diego, CA, July 29-August 1, 1985, pp. 475-481.
12. Wills, K.G., "Improvements relating to electro-deposition", *Great Britain patent 1,283,916*, August 2, 1972.
13. Josefsson, L.G., "Analysis of longitudinal slots in rectangular waveguides", *IEEE Transactions on Antennas and Propagation*, vol. AP-35, no. 12, Dec. 1987, pp. 1351-1357.
14. Sangster, A.J., and McCormick, A.H.I., "Theoretical design/synthesis of slotted waveguide arrays," *IEE Proceedings Pt. H*, Vol. 136, No. 1, Feb. 1989.
15. Wade, P., "Rectangular waveguide to coax transition design," *QEX Magazine*, Nov/Dec 2006, pp. 10 – 17.
16. Mumford, W.W., "The optimum piston position for wide-band coaxial-to-waveguide transducers", *Proceedings of the IRE*, Feb 1953, pp. 256 – 261.
17. Demotte, P., "Waveguide-coaxial line transitions", *Belgian Microwave Roundtable*, 2001, pp. 1–12.
18. Ponchak, G.E., and Downey, A.N., "A new model for broadband waveguide to microstrip transition design", *NASA Technical Memorandum 88905*, December 1986.
19. Gaudio, J.G., and Debski, T.R., "Broadband waveguide to coaxial transition", *United States Patent 3,737,812*, June 5, 1973.
20. Tadachi, A., and Sato, M., "Waveguide-to-coaxial converter," *United States Patent 4,652,839*, March 24, 1987.

21. Burger, S., and Oberle, K.P., "Device for fastening an excitation element in a metal waveguide of an antenna and for electrically connecting the same to a coaxial line arranged outside the waveguide", *United States Patent 6,088,001*, July 11, 2000.
22. Deshpande, M.D., Das, B.N., and Sanyal, G.S., "Analysis of an end launcher for an X-band rectangular waveguide", *IEEE Transactions on Microwave Theory and Techniques*, Vol. MTT-27, No. 8, August, 1979, pp. 731-735.
23. Ko, Y.H., "Final Report: Development of planar array antennas for DBS using slotted waveguide," Mt. Crane Open Joint Technology Development Project, Chonbuk National University, 19th February, 1990.
24. http://www.feko.info/
25. http://www.cst.com/Content/Products/MWS/Overview.aspx
26. http://www.ansoft.com/products/hf/hfss/
27. Brown, K.W., "Design of waveguide slotted arrays using commercially available finite element analysis software", *IEEE Antennas and Propagation Symposium*, 1996, pp. 1000-1003.
28. Hamadallah, M., "Frequency Limitations on Broad-Band Performance of Shunt Slot Arrays", *IEEE Transactions on Antennas and Propagation*, Vol. 37, No. 7, July 1989, pp. 817-823.
29. Lyon, R.W., and Sangster, A.J., "Efficient moment method analysis of radiating slots in a thick-walled rectangular waveguide," *IEE Proceedings Part H*, Vol. 128, No. 4, Aug. 1981, pp. 197-205.
30. Stegen, R.J., "Longitudinal shunt slot characteristics", *Hughes Aircraft Company, Technical Memorandum no. 261*, Nov. 1951.
31. Elliot, R.S., and Kurtz, L.A., "The design of small slot arrays", *IEEE Transactions on Antennas and Propagation*, vol. 26, no. 2, March 1978, pp. 214-219.
32. Coetzee, J.C., and Joubert, J., "The effect of the inclusion of higher order internal coupling on waveguide slot array performance", *Microwave and Optical Technology Letters*, Vol. 17, No. 2, Feb. 5, 1998, pp. 76-81.
33. A. Bojovschi, K. J. Nicholson, A. Galehdar, P. J. Callus, and K. Ghorbani, "The Role of Fibre Orientation on the Electromagnetic Performance of Waveguides Manufactured from Carbon Fibre Reinforced Plastic," *Progress In Electromagnetics Research*, vol. 39, pp. 267–280, 2012.
34. Erlinger, J. J., and Orlow, J. R., "Waveguide Slot Array with CSC^2 - COS Pattern," *Proceedings of the 1984 Antenna Applications Symposium*, Urbana, Illinois, USA, 19-21 September 1984, pp. 83-112.
35. Kaminow, I. P., and Stegen, R. J., "Waveguide Slot Array Design," *Technical Memorandum No. 348*, Hughes Aircraft Company, 1 July 1954.
36. Wade, P., "Rectangular waveguide to coax transition design," *QEX*, November, 2006.

DEFENCE SCIENCE AND TECHNOLOGY GROUP DOCUMENT CONTROL DATA			1. DLM/CAVEAT (OF DOCUMENT)
2. TITLE Methods of Designing and Feeding Carbon Fibre Reinforced Plastic Slotted Waveguide Antenna Arrays		3. SECURITY CLASSIFICATION (FOR UNCLASSIFIED LIMITED RELEASE USE (U/L) NEXT TO DOCUMENT CLASSIFICATION) Document (U) Title (U) Abstract (U)	
4. AUTHOR(S) Derek Gray, Kelvin J. Nicholson, Kamran Ghorbani, and Paul J. Callus		5. CORPORATE AUTHOR Defence Science and Technology Group 506 Lorimer St. Fishermans Bend Victoria 3207 Australia	
6a. DST GROUP NUMBER DST-Group-TR-3424	6b. AR NUMBER AR-017-017	6c. TYPE OF REPORT Technical Report	7. DOCUMENT DATE April 2018
9.TASK NUMBER ERP 07/292	10.TASK SPONSOR Chief, Air Vehicles Division	10. RESEARCH DIVISION Aerospace Division	
11. MSTC Airframe Technology & Saftey		12. STC Advanced Composite Technologies	
15. SECONDARY RELEASE STATEMENT OF THIS DOCUMENT *Approved for public release* OVERSEAS ENQUIRIES OUTSIDE STATED LIMITATIONS SHOULD BE REFERRED THROUGH DOCUMENT EXCHANGE, PO BOX 1500, EDINBURGH, SA 5111			
16. DELIBERATE ANNOUNCEMENT No limitations			
17. CITATION IN OTHER DOCUMENTS Yes			
18. RESEARCH LIBRARY THESAURUS Antenna design, Antenna radiation patterns, Carbon fibre reinforced composites, Composite structures			
19. ABSTRACT This report describes the ongoing development of the Slotted Waveguide Antenna Stiffened Structure (SWASS) technology during the period 2010 to 2012. In SWASS, blade stiffeners in sandwich panels or top-hat stiffeners on skins serve the dual purpose of providing both structural reinforcement while acting as radiofrequency waveguides. Slots cut through the outer skin and into the waveguides produce slotted waveguide antenna arrays. The development and validation of a radiofrequency design methodology, based on the finite element method, for resonant slotted waveguide antenna arrays, is described. This methodology was used to design seven-slot and ten-slot arrays that were subsequently machined into waveguides manufactured from aluminium alloy and aerospace grade carbon fibre reinforced plastic (CFRP). Additionally, the performance of a plug-and-loop radiofrequency feeding method for resonant SWASS waveguides is analysed.			